Monitoring of wheat crops using the backscattering coefficient and the interferometric coherence derived from Sentinel-1 in semi-arid areas

Nadia Ouaadi, Lionel Jarlan, Jamal Ezzahar, Mehrez Zribi, Saïd Khabba, Elhoussaine Bouras, Safa Bousbih, Pierre-Louis Frison

Monitoring of wheat crops using the backscattering coefficient and the interferometric coherence derived from Sentinel-1 in semi-arid areas

Nadia Ouaadi[a,b,*], Lionel Jarlan[b], Jamal Ezzahar[c,d], Mehrez Zribi[b], Saïd Khabba[a,d], Elhoussaine Bouras[e,b], Safa Bousbih[f], Pierre-Louis Frison[g]

[*]corresponding author

[a]LMFE, Department of Physics, Faculty of Sciences Semlalia, Cadi Ayyad University, Marrakech, Morocco.

[b]CESBIO, University of Toulouse, IRD/CNRS/UPS/CNES, Toulouse, France.

[c] MISCOM, National School of Applied Sciences, Cadi Ayyad University, Safi, Morocco.

[d]CRSA, Mohammed VI Polytechnic University UM6P, Benguerir, Morocco.

[e]ProcEDE, Department of Applied Physique, Faculty of Sciences and Technologies, Cadi Ayyad University, Marrakech, Morocco.

[f]INAT, GREEN-TEAM, Tunis, Tunisia.

[g]LaSTIG//MATWAS, IGN, University of Paris-Est, Champs sur Marne, Paris, France.

nadia.ouaadi@gmail.com

lionel.jarlan@ird.fr

j.ezzahar@uca.ma

mehrez.zribi@cesbio.cnes.fr

khabba@uca.ac.ma

bouras.elhoussaine@gmail.com

safabousbih1@outlook.fr

pierre-louis.frison@u-pem.fr

Keywords

Sentinel-1, Surface soil moisture, Backscattering coefficient, C-band, Interferometric coherence, Winter wheat, Semi-arid region.

Abstract

Radar data at C-band has shown great potential for the monitoring of soil and canopy hydric conditions of wheat crops. In this study, the C-band Sentinel-1 time series including the backscattering coefficients σ^0 at VV and VH polarization, the polarization ratio (PR) and the interferometric coherence ρ are first analyzed with the support of experimental data gathered on three plots of irrigated winter wheat located in the Haouz plain in the center of Morocco covering five growing seasons. The results showed that ρ and PR are tightly related to the canopy development. ρ is also sensitive to soil preparation. By contrast, σ^0 was found to be widely linked to changes in surface soil moisture (SSM) during the first growth stages when Leaf Area Index remains moderate (<1.5 m^2/m^2). In addition, drastic changes in the crop geometry associated to heading had a strong impact on the C-band σ^0, in particular for VH polarization. The coupled water cloud and Oh models (WCM) were then calibrated and validated on the study sites. The comparison between the predicted and observed σ^0 yielded a root mean square error (RMSE) values ranging from 1.50 dB to 2.02 dB for VV and between 1.74 dB to 2.52 dB for VH with significant differences occurring in the second part of the season after heading. Finally, new approaches based on the inversion of the WCM for SSM retrieval over wheat fields were proposed using Sentinel-1 radar data only. To this objective, the dry above-ground biomass (AGB) and the vegetation water content (VWC) were retrieved from the interferometric coherence and the PR. The relationships were then used as the vegetation descriptor in the WCM. The best retrieval results were obtained using the relationship between ρ_{VV} and the AGB (R and RMSE of 0.82, 0.05 m^3/m^3 respectively and no bias). The new retrieval approaches were then applied to a large database covering a rainfed field in Morocco and 18 plots of rainfed and irrigated wheat of the Kairouan plain (Tunisia) and compared to other classical techniques of SSM retrieval including simple linear

relationships between SSM and σ^0. The method based on the WCM and the ρ_{VV}-AGB relationships also provided with slightly better results than the others on the validation database (r=0.75, RMSE=0.06 m^3/m^3 and bias=0.01 m^3/m^3 over the 18 plots of Tunisia) but the simple linear relationships performed also reasonably well (r=0.62, RMSE=0.07, bias=-0.01 in Tunisia for instance). This study opens perspectives for high resolution soil moisture mapping from Sentinel-1 data over south Mediterranean wheat crops and *in fine*, for irrigation scheduling and retrieval through the assimilation of these new products in an evapotranspiration model.

Introduction

In the semi-arid regions where the water resources are very limited and where up to 90% of the available water is used for irrigation, surface soil moisture (SSM) is a key parameter for crop water stress detection and for irrigation management. Wheat crop is of prime importance as it represents the most cropped cereal in the world, and particularly in Morocco where 75% of the useful agricultural area are dedicated to wheat (Ministre de l'agriculture et peche maritime du develpement rurale et des eaux et forets, 2018). Several global soil moisture products exist nowadays. They are derived from microwave remote sensing including active sensors such as: scatterometers (Naeimi et al., 2009; Wagner et al., 1999) or radiometers like the Soil Moisture and Ocean Salinity mission -SMOS- (Kerr et al., 2001) or the Advanced Microwave Scanning Radiometer -AMSR- (Njoku, 2004). The potential of microwave data in this context originates from their high sensitivity to changes of surface parameters including the SSM, the soil roughness, the above ground biomass (AGB) and the canopy geometry. In addition, microwave signal at these wavelengths is not prone to atmospheric perturbation which is a major advantage with regards to optical data. However, soil moisture products derived from scatterometers or microwave radiometers suffers from a coarse spatial resolution above 10 km^2 not suited for a fine monitoring of crops at the field scale. By contrast, SAR (Synthetic Aperture Radar) observations are acquired with a pixel of around 10 m but the use of such data to monitor operationally soil moisture was still limited until the recent launch of the Sentinel-1 constellation that opened new perspectives for the monitoring of crops at the field scale by providing high resolution (10 m) data with revisit time of about 6 days at C-band (Torres et al., 2012).

The numerous theoretical and experimental studies carried out during the 80s and the 90s demonstrated the richness of information contained in the C-band signal but also the

complexity of interpreting the time series. Indeed, for annual crops like wheat, contributions to the signal from the soil and from the vegetation are merged and are changing quickly. The co-polarizated (HH and VV) backscatter coefficient are usually preferred for soil moisture retrieval (Bai et al., 2017; Gherboudj et al., 2011; Zribi et al., 2011) while some studies revealed that the cross-polarized (VH and HV) data was better suited for vegetation monitoring including both classification and biomass retrieval (Hosseini and McNairn, 2017). Indeed, over bare soils, the backscattering coefficient σ^0 is affected by the dielectric properties of the superficial layer of the soil mainly governed by SSM, and, to a lesser extent, soil texture (Dobson and Ulabz, 1981; Ulaby et al., 1986) and by the soil roughness (Ferrazzoli et al., 1992; Ulaby et al., 1978; Zribi and Baghdadi, 2015). Considering the sensitivity to SSM, several retrieval algorithms based on C-band data have been developed on bare soils. They were empirically based taking advantage of the linear relationships between σ^0 and SSM (Amazirh et al., 2018; Griffiths and Wooding, 1996; Moran et al., 1997; Sano et al., 1998; Zribi et al., 2003; Zribi and Dechambre, 2002) or they relied on the inversion of a soil backscattering model (Baghdadi et al., 2008; Bertuzzi et al., 1992; Bindlish and Barros, 2000; Ezzahar et al., 2020; Walker et al., 2004). For vegetated surface, the signal at C-band is a complex mix of a soil contribution attenuated by the canopy, of the volume scattering within the canopy and of the interactions between soil and vegetation (Ulaby et al., 1986). In order to separate soil and vegetation contributions, the retrieval of SSM over vegetated terrain is thus usually carried out using a model predicting the interaction between the electromagnetic wave and the different surface elements. Within this context, several backscattering models were developed (Attema and Ulaby, 1978; Karam et al., 1995, 1993, 1992; Picard and Toan, 2002; Ulaby et al., 1990) with the aim to get a better understanding of the response of vegetation and soils and to be used within an inversion

process (Balenzano et al., 2011; Brisco et al., 1990; Mattia et al., 2003; Picard et al., 2003). Among backscattering models of various complexity, the semi-empirical water cloud model (WCM) (Attema and Ulaby, 1978) based on the first order solution of the radiative transfer equations has been extensively used as it represents a good trade-off between domain of validity and model complexity as response of the vegetation canopy is parameterized thanks to two parameters only. Coupled to a soil backscattering model, it has been widely used for SSM and biophysical parameters retrieval especially for crops such as wheat (Baghdadi et al., 2017; Bai et al., 2017; Bindlish and Barros, 2001; Bousbih et al., 2017; El Hajj et al., 2016; Gherboudj et al., 2011; Hosseini and McNairn, 2017; Periasamy, 2018; Taconet et al., 1994; Ulaby et al., 1984; Wang et al., 2018; Zribi et al., 2011). To describe vegetation development within the water cloud model, several variables have been proposed. Most of published studies used preferentially Vegetation Water Content (Attema and Ulaby, 1978; Bindlish and Barros, 2001; Wang et al., 2018) but Prevot et al. (1993) argued that there is no general theoretical framework to define the best set of canopy descriptors in the WCM because the complexity of the vegetation's structure and of the relative simplicity of the model. Within this context, a few authors proposed different descriptors: plant height (Kumar et al., 2015), HV backscattering coefficient (Li and Wang, 2018), polarization ratio (Dabrowska-Zielinska et al., 2018), Radar Vegetation Index (Li and Wang, 2018) or LAI (Leaf Area Index) (Bai et al., 2017; El Hajj et al., 2016; Kumar et al., 2014; Prevot et al., 1993). With the recent launch of Sentinel-2, a lot of recent studies used optical-derived descriptors such as NDVI (Normalized difference vegetation index) (Baghdadi et al., 2017; Bousbih et al., 2017; El Hajj et al., 2016) that is related to vegetation greenness. Nevertheless, a severe lack of observations may occur in case of a persistent cloud cover which is very likely when wheat is cropped during the rainy season such as in the South Mediterranean region.

137 The radar interferometric coherence is defined as the variance of the interferometric phase,
138 which is related to the path length between the satellite antenna and the ground target. It is
139 related to the amount of coherent and incoherent scattering. Beside the system noise, the
140 coherence decreases with increasing volume scattering, because of target changes between
141 two successive radar acquisitions or because of the natural motion of the scatterers (Zebker
142 and Villasenor, 1992). State differently, volume scattering and arbitrary dislocation of
143 scatterers in the vegetation canopy reduce the coherence. Even if dry fields exhibit lower
144 interferometric coherence than wet fields (Blaes and Defourny, 2003; Nesti et al., 1998), the
145 interferometric coherence is relatively insensitive to soil effects considering that surface
146 roughness of crops does not change significantly between seeding and harvest. Wegmuller
147 and Werner (1997) found a strong correlation between the interferometric coherence and
148 the cover fraction opening perspectives for crop height and biomass estimation. Strong
149 relationships have been established between interferometric coherence at C-band and crop
150 height for some agricultural crops (winter wheat, potato, sugar beet…) at the beginning of
151 the growing season (Blaes and Defourny, 2003; Engdahl et al., 2001). Likewise, the ratio
152 HH/VV was also shown to be related to aboveground biomass during the growing season,
153 especially at 40° of incidence (Mattia et al., 2003). Since this ratio was not available in the
154 Sentinel-1 IW acquisition mode, Veloso et al. (2017) used the VH/VV backscattering ratio as a
155 solution that can reduce the vegetation-ground interaction effect as well as the errors
156 associated to the acquisition. VH/VV appears more stable in time than VH or VV and more
157 sensitive to the wheat growth cycle. Furthermore, it was correlated to the fresh biomass and
158 able to discriminate cereals from non-cereals surface dominated crops (Mattia et al., 2015;
159 Veloso et al., 2017).

160 This study presents a new SSM retrieval approach based on Sentinel-1 data only to describe
161 the vegetation contribution in the WCM. The approach is developed on two monitored
162 irrigated wheat fields located in Morocco and evaluated on a large database covering 20
163 rainfed and irrigated plots in Morocco and Tunisia. The next section describes the satellite
164 and the *in situ* measurements, the backscattering models and the retrieval algorithm.
165 Results are presented in section 3 including the experimental analysis of Sentinel-1 time
166 series, the forward modeling of the backscattering coefficient and the SSM retrieval. In
167 section 4, the main conclusions and perspectives are drawn.

168

1. Experimental data and Methodology

1.1. Experimental data

The SSM retrieval approaches were developed on three irrigated wheat plots located near Chichaoua city that were intensively monitored during two crop seasons. A database of soil moisture measurements on rainfed and irrigated wheat in Morocco and Tunisia described in section 1.1.3 was gathered to validate the approach.

1.1.1. Study area description

The study site is located in the province of Chichaoua at 65 Km west of Marrakech city in the Haouz plain center of Morocco (Fig. 1). The region is characterized by a semi-arid Mediterranean climate. The annual average precipitation amount is about 250 mm (Ait Hssaine et al., 2018; Rafi et al., 2019). The monthly average of rainfall distribution measured at Chichaoua shows the existence of two characteristic periods: a wet season from October to April (85-89% of the annual amount) and a dry season from May to September (11- 15%). The average maximum temperature occurs in July-August (27.2°C) while the minimum (10.8°C) is in January. The reference evapotranspiration ET_0 is about 1600 mm (Jarlan et al., 2015).

Two fields, named Field 1 and Field 2 (Fig. 1), of about 1.5 ha each, were selected within a private farm named “Domaine Rafi” and monitored during two crop seasons from November 2016 to July 2018. Soil texture is mainly clay (37.5%) and sand (32.5%). Field 1 and Field 2 were seeded with winter wheat on November, 27, 2016 and November, 25, 2017 for 2016-2017 and 2017-2018 crop seasons, respectively. Harvest occurred on May, 16, 2017 and June, 08, 2018. The irrigation method used is the drip technique with a flow rate of 7.14 mm/hour for each dripper. Field 2 was irrigated according to FAO recommendations while

192 Field 1 suffered from a triggered stress for the need of another research study (Ait Hssaine
193 et al., 2018; Rafi et al., 2019). After harvest, the fields were used as cattle grazing up to mid-
194 July when the plowing works started. Please note that wheat growth on Field 2 during the
195 2017-2018 growing season was severely affected by very specific growing conditions: (1)
196 very invasive adventices with a strong horizontal development (cf picture S1 in the
197 supplementary material). The adventices species belong to the family of wild thistles that is
198 not very widespread on wheat fields in the South Mediterranean area (Tanji, 2005). Some
199 part of the field were almost completely covered around vegetation peak; (2) Field 2 during
200 the second year was more exposed to wind than Field 1 because the density of seeding was
201 much higher and because a mix of wheat and barley were seeded by mistake. Barley is
202 characterized by longer stems than wheat that grown up to 146 cm on April 2018 thanks to
203 irrigation. By contrast, the height of stems on Field 1 seeded with pure wheat, only reached
204 110 cm. Stems were almost completely laid down by the wind from April 12, 2018 (see
205 picture S2) on Field 2. Considering these very specific growing conditions of Field 2 during
206 the 2nd year, a third field named Field 3 (Fig. 1), was also instrumented during 2018-2019 to
207 extent the validation database under normal growing conditions. It was seeded on
208 November 4, 2018 and harvested on June 06, 2019. Field 3 has the same soil as Field 1 and 2
209 and is also watered by drip irrigation.

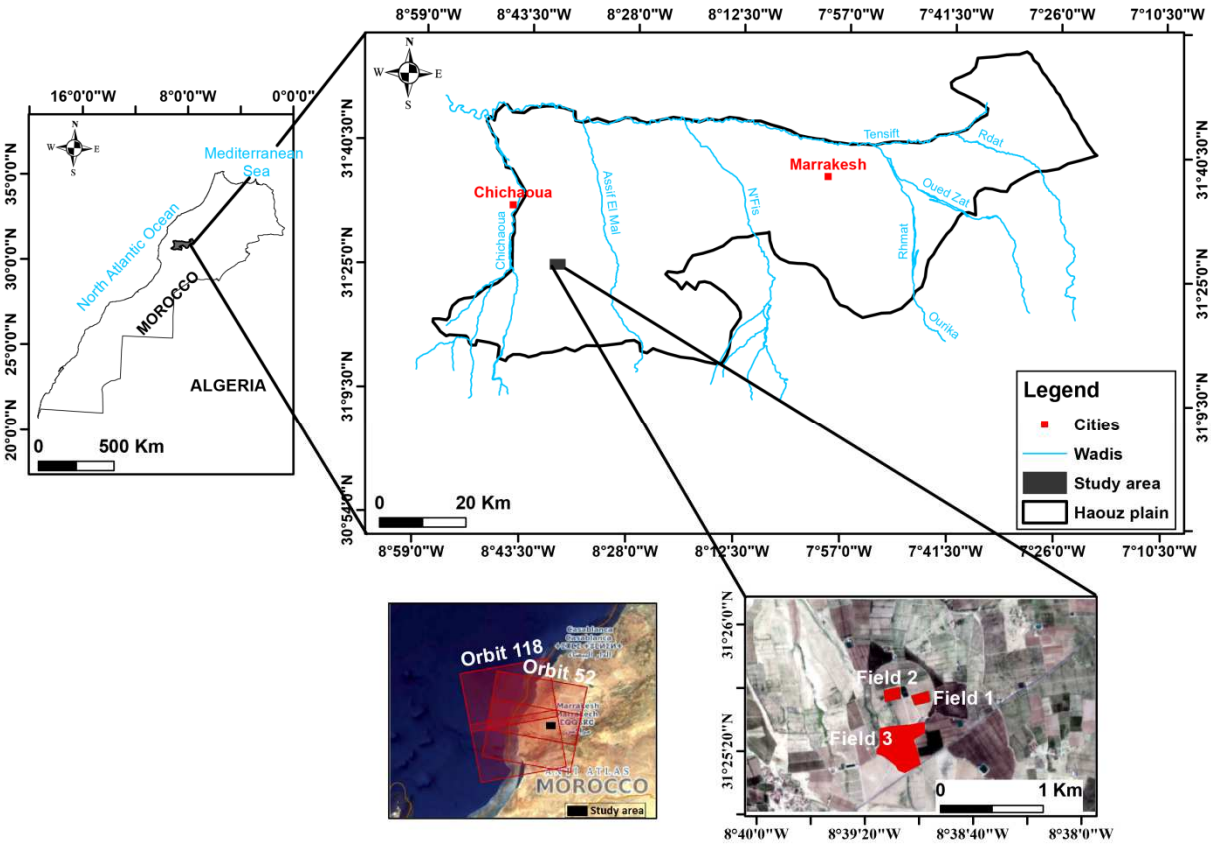

210

211 *Fig. 1. Location of the study sites: Field 1 (stressed), Field 2 (reference) and Field 3 drip-irrigated wheat crops near*
212 *Chichaoua city in a private farm ("Domaine Rafi"), west of Marrakech, Haouz plain, center of Morocco.*

213 ### 1.1.2. Field data description

214 Vegetation and soil measurements were collected according to the Sentinel-1 passage
215 schedule. The days corresponding to precipitation events were discarded.

216 *Soil measurements*

217 Automatic measurements of SSM were acquired at a 30 min time step from Time Domain
218 Reflectometry sensors (TDR Campbell Scientific CS616) buried at a depth of 5 cm. In order
219 to get a measurement representative of the Sentinel-1 pixel, the soil moisture observations
220 were taken as the average of two sensors data that were installed between and under the
221 drippers. The gravimetric technique was used to calibrate the TDR measurements.
222 Measurements were carried out, over Field 1 and Field 2, for five days in order to cover a

223 wide range of soil moisture values (0.08 to 0.33 m^3/m^3). Three samples were collected per
224 day and per field at the TDR installation depth using a 392.5 cm^3 aluminum core. A linear
225 regression was established between the volumetric water content and the square root of
226 the TDR time response. The corresponding RMSEs (all the statistical metrics used in this
227 study are described in the supplementary material) over Field 1 and Field 2 are 0.023 m^3/m^3
228 and 0.010 m^3/m^3, respectively. The same relationship was applied to Field 3 data.

229 Soil roughness corresponds to micro-topographic variations of the soil surface. It was
230 measured once a week during the first stages of wheat development until the canopy
231 prevented from making the measurement (corresponding to a canopy fraction cover of
232 about 0.8). A pin profiler of 1 m length with 2 cm between two successive needles was used.
233 For Field 1 and Field 2, sixteen samples at different places were taken per field including
234 eight measurements made parallel to the row and eight perpendicular in order to take into
235 account the effect of the rows direction (Sieber et al., 1982). A picture of the pin profile was
236 taken for each sample and processed using an algorithm based on the normalization of the
237 needles height. For each roughness profile, two statistical parameters used as inputs of the
238 backscattering soil models were derived from the correlation functions of the heights of the
239 surface profiles: the root mean square surface height (h_{rms}) and the correlation length (L)
240 (Nolin et al., 2005). For each date and each field, an average of h_{rms} and L is computed from
241 the 16 sample estimates. h_{rms} and L values ranged from 0.7 to 1.5 cm and 4.8 to 7.3 cm,
242 respectively. A preliminary analysis of the time series of h_{rms} and L values show that the
243 values are quite similar for measurements parallel and perpendicular to the row apart from
244 the beginning of the season when rows are still clearly visible because of the sowing (not
245 shown). This anisotropy disappeared quickly with irrigation and plant growth. The average of
246 h_{rms} and L for all the measurements in each direction are reported in Table 1. The values are

of the same order of magnitude for Field 2 while a slight difference is observed for Field 1. For reasons of simplicity, the surface roughness is considered isotropic in this study.

Table 1
h_{rms} and L average values for measurements parallel and perpendicular to the row over Field 1 and Field 2.

	Field 1				Field 2			
	Parallel		Perpendicular		Parallel		Perpendicular	
	h_{rms}(cm)	L (cm)	h_{rms} (cm)	L (cm)	h_{rms} (cm)	L (cm)	h_{rms}(cm)	L (cm)
Average	0.95	5.20	1.26	6.53	1.15	5.82	1.16	6.17

Wheat measurements

In the presence of vegetation canopy, the microwave backscattering is significantly related to vegetation's parameters such as biomass, plant water content and geometry (Ferrazzoli et al., 1992; Ulaby et al., 1986). Destructive above-ground biomass (AGB) measurements were conducted about every 15 days. Plant sampling was conducted in eight quadrates (0.25m*0.25m) selected randomly in each field. The AGB is weighted first in the field (hereafter named fresh above ground biomass or FAGB). The samples were then dried in an oven at 105°C for 48 h. The weighted samples after drying are used to compute the AGB expressed in kg of dry matter by m^2. The difference between wet and dry samples is the vegetation water content (VWC). The canopy fraction cover (Fc) and the leaf area index (LAI) were calculated by processing eleven hemispherical digital images per field, taken every week at various representative points and by computing the average of individual pictures. The canopy height was also measured by averaging eleven measurements per field.

Meteorological data

A complete automatic weather station installed over an alfalfa field near the study site provided continuous measurements of meteorological forcing, including air temperature and

268 rainfall. The data were collected half-hourly, the temperature values were averaged at a
269 daily time step and the precipitation measurements were summed up to obtain daily
270 amounts.

271 ### 1.1.3. Validation database

272 SSM measurements using TDR and hand-held thetaprobe were carried out on different
273 wheat sites in Morocco and Tunisia, respectively. This database is used for the validation of
274 the retrieval approach presented in this study. Data were collected from: i) one rainfed
275 wheat located about 40 km east of Marrakech near the city of Sidi Rahal (hereafter named
276 "Sidi Rahal") during two growing seasons (2016-2017 and 2017-2018; (Amazirh et al., 2018;
277 Ezzahar et al., 2020); ii) 18 plots located in the Kairouan plain in Tunisia during the 2016-
278 2017 growing season (Bousbih et al., 2017). General information about all plots is provided
279 in Table 2. Over the Moroccan field, measurements are taken every 30 min thanks to the
280 TDR probes while 20 thetaprobe samples are averaged per field for the Tunisian plots at the
281 time of the Sentinel-1 overpass (between 30 min before and 2h after for the ascending and
282 descending orbits, respectively). Please note that it is expected that the validation database
283 covers a large variability of wheat crop conditions representative of the south
284 Mediterranean area. Indeed, it covers rainfed and irrigated fields with different technique
285 (sprinkler); owners are different, in particular for the 18 fields in Tunisia. Consequently, the
286 agricultural practices differ depending on the experience of the farmer. ''Domaine Rafi''
287 fields are well managed in terms of irrigation as the farmer follows the FAO-56
288 recommendation (Allen et al., 1998) while irrigated fields in Tunisia belong to different
289 smallholders farmers whose irrigation scheduling may be more empirical by lack of objective
290 scientific information. Likewise, nutrient inputs are used on irrigated fields of ''Domaine

Rafi'' while no inputs are applied to rainfed fields. The soil in Tunisia covered also a large variability of texture (Bousbih et al., 2019). For Morocco, the soil at ''Domaine Rafi'' is loamy-clay (37.5% clay, 32.5% sand) while it is mainly clay (47.5% clay, 18.5% sand) on the rainfed field ''Sidi Rahal''. For the latter field, contrasted annual amount of rainfall are observed for the two crops season (204.2 mm from November to May in 2016-2017 versus 408.8 mm in 2017-2018). Finally, the range of SSM for all data extended from 4 to 50%.

Table 2
General information about the validation sites over Morocco and Tunisia.

	Crop's type	Number of plots	Irrigation system	h_{rms} (cm)	SSM (m^3/m^3)
Sidi Rahal	Winter wheat	1	Rainfed	0.95	0.04-0.39
Kairouan		6	Rainfed	0.7-1.5	0.05-0.5
		12	Sprinkler		

1.1.4. Satellite data description

1.1.4.1. Sentinel-1 radar data

Sentinel-1 (S1) is an earth observation constellation with two satellites, S1A and S1B, that were launched by the European Space Agency (ESA) in April 2014 and 2016, respectively. The two satellites carry a synthetic aperture radar, operating at C-band and provide a revisit time of six days (Torres et al., 2012). The main operational imaging mode over land surfaces is the Interferometric Wide-swath mode (IW) realizing acquisitions in VV and VH polarizations with a 250 km wide swath, and high azimuth (20 m) and ground range (5 m) resolutions (Mission and Services, 2012). Across the swath, the incidence angle ranges between 31° and 46°. Level 1 products can be directly downloaded from the Sentinel-1 Data Hub website (https://scihub.copernicus.eu/). Two products types were used in this work: GRDH (Ground Range Detected High resolution) for backscattering coefficient and SLC

(Single Look Complex) for computing interferometric coherence. Table 3 summarizes all the images used within this study.

Table 3
Characteristics of the sentinel-1 data on the calibration and validation sites.

Site	Season	Relative Orbit Number	Incidence angle	Relative Orbit	Overpass time	Product	Number of images
Field 1 & Field 2	October 2016 - July 2018	118 & 52	45,6° & 35,2°	Ascending & Descending	18:30 & 06:30	GRD SLC	207 219
Field 3	November 2018 - Mai 2019	118 & 52	45,6° & 35,2°	Ascending & Descending	18:30 & 06:30	GRD SLC	65 65
Sidi Rahal	November 2016-June 2017 &November 2017-June 2018	154	40°	Descending	06:28	GRD SLC	61 60
Kairouan	November 2016- April 2017	88 & 95	39,5°-40°	Ascending & Descending	17:20 & 05:21	GRD SLC	14 14

GRD products processing: the backscattering coefficient

GRD images product were processed using the Orfeo ToolBox (OTB) (CNES, 2018) at the original 10 m resolution to obtain the backscattering coefficients σ^0. Three processing steps were applied: i) Thermal noise removal; ii) Calibration (Miranda et al., 2015); iii) Terrain correction (Small, 2011) using the DEM SRTM (Shuttle Radar Topography Mission) at 30 m resolution according to the method described in Small and Schubert (2008). In order to minimize speckle effects, a simple spatial average is performed at the field scale. For instance, the σ^0 of Field 1 and Field 2 are average values computed from 120 and 121 pixels, respectively. The standard deviation is also computed for each field and each acquisition time. Finally, the polarization ratio $\sigma^0_{VH}/\sigma^0_{VV}$ (PR) is computed.

SLC products processing: the interferometric coherence

Sentinel-1 Level 1 SLC products provide data in slant-range geometry and contain phase and amplitude information. The interferometric coherence was calculated from two consecutive acquisitions of the same orbit (*i.e.* 6 days with S1A and S1B) by cross multiplying pixel by pixel the first SAR image with the complex conjugate of the second (Bamler and Hartl, 1998; Touzi et al., 1999) for a given local neighborhood (in this study, 3*15 was used in order to get a square pixel).

The amplitude $|\rho|$, named coherence, ranges between 0 (incoherence) and 1 (perfect coherence). It characterizes the stability of the scatterers at the scale of the wavelength within the same cell. The coherence decreases when changes of scatterers geometrical properties (position, orientation, …) occur. Consequently, it is expected to be low in the case of dense vegetation and strong on bare rocky soils. Over vegetation, the random dislocation of scatterers because of weather (wind and rain) or because of the plants growth is the main cause of the temporal decorrelation.

The Sentinel application platform SNAP was used to calculate the coherence in 5 steps: (1) The "Apply-Orbit-file" module for a better estimation of the position and speed of the satellite; (2) the two images were co-registered ("Back-geocoding") using the orbital data and the DEM SRTM; (3) The "Coherence" module was applied (4) the bursts (black band in the SLC products) were deleted by applying the "TOPSAR-Deburst" module; (5) finally, "Terrain-Correction" was used to project the images on the earth surface using the SRTM DEM.

1.1.4.2. Sentinel-2 optical data

ESA's optical Sentinel-2 satellites S2A and S2B were also launched on June 2015 and March 2017, respectively. Sentinel-2 provides images every 5 days for 13 spectral bands at a resolution ranging from 10 to 60 m according to the spectral band. Level 2A images were processed and provided by the National Centre for Space Studies (CNES) through the PEPS platform free of charge within the frame of THEIA (https://theia.cnes.fr/). Data were corrected from atmospheric effects using the MAJA processor designed at CESBIO (Hagolle et al., 2015). 10 of the 17 images (S2A) were cloud-free for the first agricultural season (November 2016 to May 2017) while 25 products were retained among 33 available for the second season (November 2017 to June 2018) on the two fields (Field 1 and Field 2) of "Domaine Rafi". The NDVI was computed from individual bands 4 and 8 and averaged over each field. Standard deviation of NDVI for each field and each date is also computed.

1.2. Backscatter modeling

In order to deepen our understanding of the signal, and for the SSM retrieval, a modeling approach was implemented. Semi-empirical and empirical approaches were preferred here to complex physically based models such as Karam et al. (Karam et al., 1992) or MIMICS (Ulaby et al., 1990) as their use within an inversion scheme is still difficult because of their complexity and their large number of input parameters. Within this study, the simple semi-empirical water cloud model (Attema and Ulaby, 1978) representing the vegetation canopy as a cloud of identical water droplets for vegetation backscattering coupled to the empirical Oh et al. (1992) model for the underlying soil was chosen. A short description of the models is provided in the appendix 1. The coupled models hereafter called WCM links the backscattering coefficient to the two empirical parameters A_{pq} and B_{pq} (Equ. A8 and A9)

and a vegetation descriptor for the WCM and the standard deviation of the surface height h_{rms} and the SSM for Oh et al.

1.3. Surface soil moisture retrieval

Several approaches based on the inversion of the water cloud model for SSM retrieval have been already proposed using different vegetation descriptor: VWC (Attema and Ulaby, 1978; Bindlish and Barros, 2001; Wang et al., 2018), AGB (Hosseini and McNairn, 2017), LAI (Bai et al., 2017; Kumar et al., 2014; Prevot et al., 1993) or NDVI (Baghdadi et al., 2017; Bousbih et al., 2017; El Hajj et al., 2016). In this study, a new approach is proposed based on the interferometric coherence that has already been shown to be tightly related to vegetation characteristic (Blaes and Defourny, 2003; Engdahl et al., 2001; Wegmuller and Werner, 1997).

As a preliminary step, a relation was first sought between Sentinel-1 variables and *in situ* measurements of vegetation characteristics (VWC and AGB). The WCM was calibrated on the two irrigated wheat fields (cf. section 2.2) of "Domaine Rafi" (Field 1 and Field 2) using the measured vegetation characteristics, soil roughness and SSM. The calibration was repeated twice using AGB and VWC. Then, for the retrieval of SSM, the relationships between interferometric coherence and vegetation characteristics were used as input of the calibrated WCM providing with two different inversion approaches called $\mathrm{WCM}_{\rho-\mathrm{AGB}}$ and $\mathrm{WCM}_{\rho-\mathrm{VWC}}$. SSM time series were retrieved by minimizing the distance between observed and predicted backscattering coefficient for each Sentinel-1 acquisition. VV and VH polarizations were tested. The minimization was carried out using a simple "brute-force" approach (Jarlan et al., 2002) consisting in exploring all SSM values from 0 to 0.5 m^3/m^3 with a step of 0.0005 m^3/m^3. SSM time series retrieval is repeated for different soil roughness.

After soughing and until the next soil work occurring after harvest, it is assumed that the soil roughness of wheat crops doesn't change. The measurements carried out on the two irrigated wheat fields show that the variation of the h_{rms} parameter around its average value reached 17% for Field 1 in 2016-2017 but remained below 10% for Field 2 and the other seasons. In addition, it is also assumed that h_{rms} variability from one field to another is small considering also the period from sowing to harvest. Within this context, a constant h_{rms} is sought for the whole crop season with h_{rms} values varying from 0.7 cm to 1.5 cm with a step of 0.05 cm. The range of h_{rms} has been determined from the *in situ* database and from a literature review (Balenzano et al., 2011; Bousbih et al., 2017; Mattia et al., 2003; Picard et al., 2003; Wang et al., 2018; Zribi et al., 2011). The average of all the retrieved SSM time series is then kept as the solution to the inverse problem. Please note that a constant value of 1 cm was first used. Keeping the average of SSM time series corresponding to different values of soil roughness provided with slightly lower biases (not shown) than with the unique h_{rms} value of 1 cm.

As a significant additional processing and storage are needed to derive Sentinel-1 coherence, the added-value of using the interferometric coherence is evaluated by comparison to the same approach but based on the PR as it is also well known to be related to vegetation development (Greifeneder et al., 2018; Paloscia et al., 2013; Veloso et al., 2017). The two approaches based on the relationships between PR and vegetation characteristics are named $\mathrm{WCM}_{\mathrm{PR-AGB}}$ and $\mathrm{WCM}_{\mathrm{PR-VWC}}$. In these configurations, SSM over wheat crops could be retrieved based on Sentinel-1 data only: the backscattering coefficient and the interferometric coherence or the PR. Finally, three more classical methods for SSM retrieval composed of two empirical approaches and one based on WCM are also implemented for comparison purposes :

- *Empirical approaches*: (1) A linear relationship between the backscattering coefficient (at VV, σ^0_{VV}, or VH, σ^0_{VH} polarization) and SSM (Holah et al., 2005; Le Hégarat-Mascle et al., 2002; Le Morvan et al., 2008; Ulaby et al., 1982); (2) A linear relationship between the relative difference of backscattering coefficient between two successive acquisitions ($\Delta\sigma^0$) of the same orbit and the corresponding difference of SSM (ΔSSM) as proposed by Balenzano et al. (2011). It has been proposed as an alternative method less sensitive to change of soil roughness that may occurs during the season. Please note that for the latter method, the SSM at the start of the crop season SSM_0 must be obtained as only relative changes of SSM between successive acquisitions are retrieved. In this study, as the method is only implemented for comparison purpose, SSM_0 is taken from the *in situ* measurements. The retrieval of SSM_0 when no measurements are available may increase the uncertainties of the SSM retrieval.

- *WCM based approach*: The NDVI is used directly as the vegetation descriptor as in numerous previous works (Baghdadi et al., 2017; Bousbih et al., 2017; El Hajj et al., 2016) and the method is named $\mathrm{WCM_{NDVI}}$.

The inputs, outputs and the parameters to be calibrated prior to the inversion process for each method are provided at Table 4. The number of algorithmic parameters to be calibrated differs significantly and ranges from 2 (σ^0, $\Delta\sigma^0$ and $\mathrm{WCM_{NDVI}}$) to 5 (approaches based on the WCM and radar observations). This means that the methods based on the PR or the interferometric coherence require additional *in situ* measurements of the vegetation characteristics by contrast with the other approaches relying on SSM data only.

For the seven methods , the data of the first season (2016-2017) over both Field 1 and Field 2 were used for calibration meaning that, for the empirical approaches, a linear relationship between σ^0 (or $\Delta\sigma^0$) and SSM (or ΔSSM) is sought for the first year of data. For the WCM based methods, the first year of data is used to calibrate: (1) the A_{pq} and B_{pq} coefficients of the WCM model by minimizing the RMSE between the predicted and the observed backscattering coefficient; (2) the empirical parameters of the relationships between coherence or PR and the vegetation characteristics. A_{pq} and B_{pq} parameters were estimated separately for each radar polarization following Baghdadi et al. (2017) and Hosseini and McNairn (2017). The second year (2017-2018) on Field 1 and 2, field 3 data and the validation database are used for validation. Please note that it was decided to keep the data from the 2nd season of Field 2 for the method evaluation when wheat faces very adverse growing conditions as already described.

Table 4
Input, output and number of parameters to be calibrated for each methods.

Method	Inputs	Outputs	Calibrated parameters
σ^0	**σ^0**	SSM	a and b / σ^0=f(SSM)
$\Delta\sigma^0$	**σ^0**	ΔSSM	a and b / $\Delta\sigma^0$=f (ΔSSM)
WCM_{NDVI}	**σ^0**, NDVI	SSM	A and B / WCM
WCM_{PR-AGB}	**σ^0**, PR	SSM	A and B / WCM a, b and c / AGB=f (PR)
WCM_{PR-VWC}	**σ^0**, PR	SSM	A and B / WCM a, b and c / VWC=f (PR)
$WCM_{\rho-AGB}$	**σ^0**, ρ	SSM	A and B / WCM a, b and c / AGB=f (ρ)
$WCM_{\rho-VWC}$	**σ^0**, ρ	SSM	A and B / WCM

			a, b and c / VWC=f (ρ)

2. Results and discussions

The first section is dedicated to the Sentinel-1 products interpretation based on the field measurements and knowledge database. The second section is devoted to the WCM calibration and to the direct predictions of the backscattering coefficient. Finally, the third section deals with the SSM inversion.

2.1. Analysis of experimental data

2.1.1. Time series interpretation

Fig. 2 displays the time series of the radar responses for orbit 52 at 35.2° incidence angle, the vegetation index from Sentinel-2 and *in situ* measurements for interpretation purposes during crop seasons 2016-2017 and 2017-2018 on Field 1. The timing of the drastic drop of VWC at the end of the season is superimposed on the time series of the interferometric coherence and of the backscattering coefficients for interpretation purpose (vertical blue line). The Fig. 3 displays the same information as Fig. 2 but for orbit 118 at 45.6° of incidence angle for Field 2. The same figures but at 35.2° for Field 2 and at 45.6° for Field 1 are provided as supplementary materials (Fig. S3 and S4).

Vegetation descriptors

Cross correlations of AGB, FAGB and VWC before and after vegetation peak are provided at Table T1 (supplementary material). NDVI and LAI exhibit a close seasonal course (Fig. 2 and 3) with almost similar peak timing. Likewise, FAGB and VWC are in-line (correlation coefficients before or after peak are always above 0.97; Table T1) but with maximum values reached around 50 days later than NDVI and LAI. By contrast, AGB (corresponding to green

and dead vegetation tissues expressed in kg dry matter/m²) is highly correlated with VWC during the first part of the season (correlation coefficients of 0.73 and 0.81 for Field 1 and 2, respectively) but the correlation coefficients drastically drop after the vegetation peak (Table T1) when stems and leaves start to dry. Total VWC being dominated by stems and leaves, it drops earlier than AGB. For Field 1 in 2016-2017, high air temperature values in March lead plants to stop the leaves development early and to start the grain filling stage. Relatively low LAI values were observed at the end of March while FAGB and AGB continue to increase afterwards and until mid-April. In terms of AGB amount, systematic higher values for Field 2 are observed because of the triggered water stress on Field 1 through sub-optimal irrigation planning. Finally, observed differences of biomass between the two seasons are related to differences in the density of seeds and to more wetter conditions for season 2017-2018.

Backscattering coefficients

Backscattering coefficients exhibit a clear seasonal signal. An increase is observed on σ^0_{VV} from beginning of October until January. At this time, the signal is dominated by the quick change of soil moisture while wheat fraction cover is still low. Afterwards, the backscattering coefficient decreases with the attenuation of the soil contribution by the canopy while wheat develops. A minimum backscatter is attained around the heading stage and the signal increases again afterwards. Although this second increase is almost nonexistent for Field 1 at 35.2° of incidence angle (Fig. 2), it is clear for the other plots (Fig. 3, S3 and S4) and it appears stronger for σ^0_{VH} than for σ^0_{VV} and at 45.6° than at 35.2°. Please note that the long plateau lasting until harvest during the second season on Field 2 is a typical behavior of a crop developing a random canopy structure, which in turn produces a significant volume scattering contribution. This is because of the specific growing conditions as already

highlighted. Under normal growing conditions, several authors have attributed the second increase to the appearance of the heads creating a wet layer at the top of the canopy (Ulaby and Bush, 1976; Mattia et al., 2003; Ulaby et al., 1986) specifically for incidence angle above 40° (Brown et al., 2003). Indeed, as most of the vegetation tissues are still wet at this time, the increase of backscatter cannot be attributed to an increase of the soil contribution in response to vegetation drying as the drastic drop of VWC occurred later in the season (see blue vertical lines in figures 2, 3, S1 and S2). The second cycle from the heading stage appeared also stronger on σ^0_{VH} because volume diffusion process attributed to the head layer triggers depolarization at this time (Picard et al., 2003; Balenzano et al., 2011). In addition, maximum σ^0_{VH} values are more related to AGB than σ^0_{VV} showing the higher sensitivity of cross polarization to vegetation elements. For instance, σ^0_{VH} values at peak are higher on Field 2 than on Field 1 because of the triggered water stress that limited crop development on Field 1 (see σ^0_{VH} time series at 45.6° on both fields during the first season as Field 2 during the 2nd season faced very adverse growing conditions). The final decrease lasts until harvest with the drying of all the vegetation elements and of the soil. The drastic increase noticed in VV and VH responses after July 11 (2016-2017 season) was concomitant with a tilling work (vertical black lines). Likewise, the signal decreased on November 22 in relation to the drop of surface roughness associated to soil preparation for seeding.

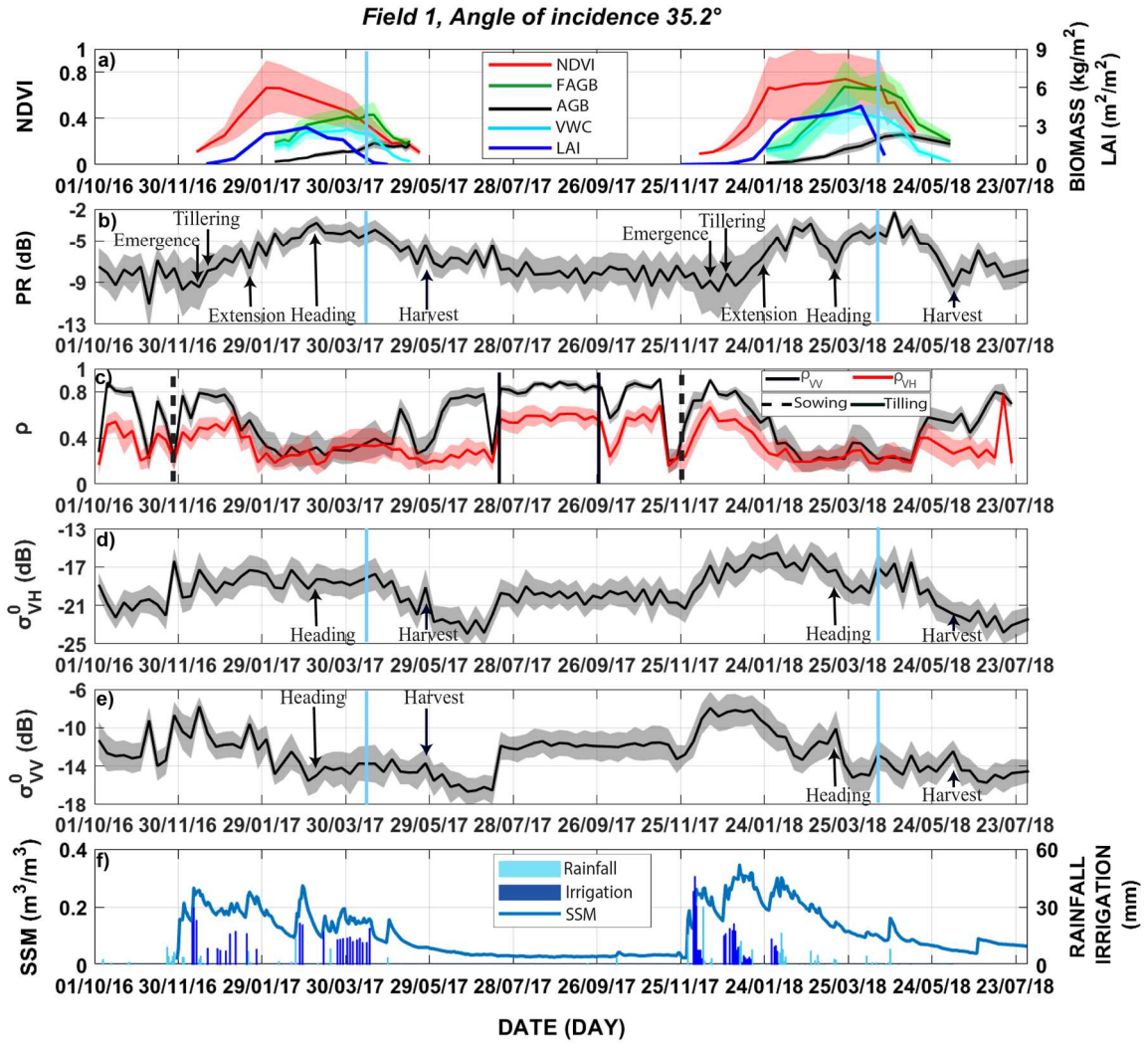

519

520 *Fig. 2. Time series of PR, σ^0_{VV}, σ^0_{VH}, ρ_{VV} and ρ_{VH} at 35.2° of incidence angle over the Field 1 and during two*
521 *agricultural seasons 2016-2017 and 2017-2018. Optical NDVI, measured LAI, measured VWC, FAGB and AGB*
522 *are plotted in the first subplot. Mean values are represented by solid lines and standard deviations by the filled*
523 *areas surrounding the curves. Rainfall, irrigation and SSM are displayed in the last subplot. Wheat phenological*
524 *stages and ground working events are superimposed. The drop of VWC at the end of the season is reported as a*
525 *blue vertical line on the time series of the polarization ratio and of the backscattering coefficients.*

526 *Polarization ratio*

527 The PR appears to be more stable than the backscattering coefficient for both polarizations
528 VV and VH. The ratio follows the evolution of FAGB. It begins to increase with the increasing
529 of biomass from the emergence until the heading, and then, both of them start to decrease
530 until harvest. For example, in Field 1 (first season), PR increases by about 9 dB from
531 emergence to heading, and peaks at the same time as biomass around mid-April. This

behavior confirms the results of previous studies (Veloso et al., 2017) and foster the use of this ratio for crop monitoring.

Interferometric coherence

VV and VH coherence exhibit similar seasonal cycle. High values of coherence (around 0.9 for VV polarization) are observed during the summer month until sowing. These high values express a dominance of coherent scattering from stable bare soils. Coherence drastically drops to about 0.15 in autumn at the time of tilling work carried out before sowing. It then gradually recovers high values (about 0.7) until emergence when it starts a slow decrease until about the extension of the stems to become almost constant (corresponding to the noise level) afterwards. As for the backscattering coefficient, this average seasonal course is disturbed by agricultural actions. The observed peak between sowing and emergence may be related to the installation of irrigation drippers that took place about two weeks after sowing on both fields. Between the harvest and the first tilling on July 11th 2017, the plots are used for cattles grazing which can explain the observed changes of coherence. The abrupt decrease noted on July 11th 2017 is owing to deep ploughing. Soil works and farming activities have already been found to induce a large decrease in coherence (Wegmuller and Werner, 1997). After this date, the VV coherence ρ_{VV} reaches its highest value of about 0.9 until the sowing of the second season. Although some authors (De Zan et al., 2014; Morrison et al., 2011; Scott et al., 2017) demonstrated a sensitivity of coherence to soil moisture, a visual inspection of the time series of coherence and soil moisture (Fig. S5 in the supplementary material) does not highlight any strong linkage between both variables. In addition, the correlation coefficients r computed between the interferometric coherence and either soil moisture or soil moisture change between the dates used to compute the

555 coherence remains below 0.20 at the seasonal scale (Table T2 in the supplementary
556 material).

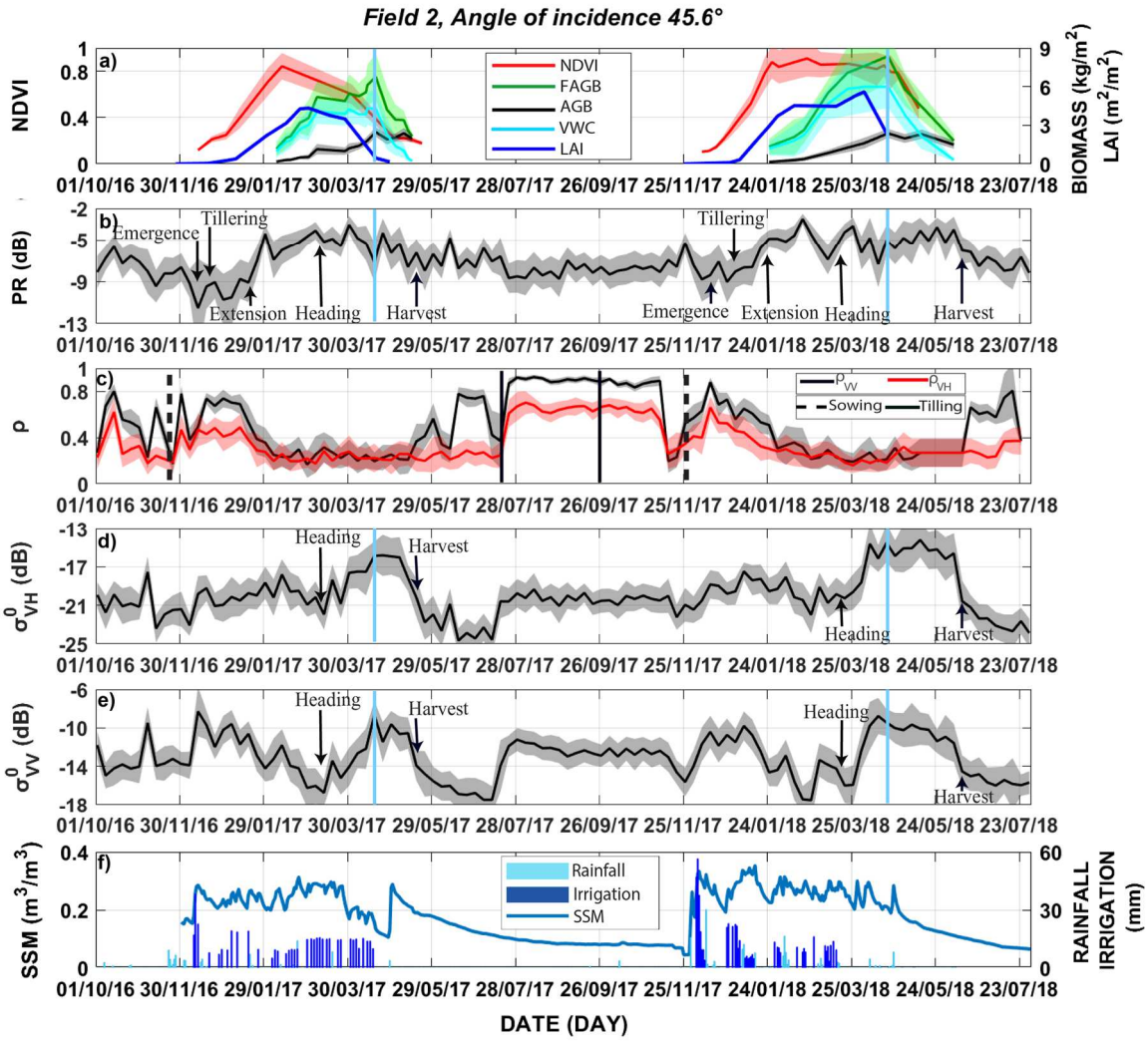

557

558 *Fig. 3. Time series of PR, σ^0_{VV}, σ^0_{VH}, ρ_{VV} and ρ_{VH} at 45.6° of incidence angle over the Field 2 and during two*
559 *agricultural seasons 2016-2017 and 2017-2018. Optical NDVI, measured LAI, measured VWC, FAGB and AGB*
560 *are plotted in the first subplot. Mean values are represented by solid lines and standard deviations by the filled*
561 *areas surrounding the curves. Rainfall, irrigation and SSM are displayed in the last subplot. Wheat phenological*
562 *stages and ground working events are superimposed. The drop of VWC at the end of the season is reported as a*
563 *blue vertical line on the time series of the polarization ratio and of the backscattering coefficients.*

564

565 ### 2.1.2. Backscattering coefficients and surface soil moisture

Fig. 4 displays the relationship between the backscattering coefficient and the SSM for VV and VH polarization at 45.6° (a and b) and 35.2° (e and f) of incidence angle, and between the difference of backscattering between two successive acquisitions and the corresponding difference of SSM (c, d, g and h). All data are represented (two fields and two seasons). Black points correspond to LAI up to 1.5 m^2/m^2 while data corresponding to LAI value above this threshold are plotted in grey. The 1.5 m^2/m^2 of LAI correspond on average to AGB≅0.14 kg/m^2 and to VWC≅1.00 kg/m^2. The statistical metrics and the equation of the superimposed linear fit are given for the whole season. Statistical metrics for LAI<1.5 and for LAI>1.5 are also reported in Table T3 of the supplementary material.

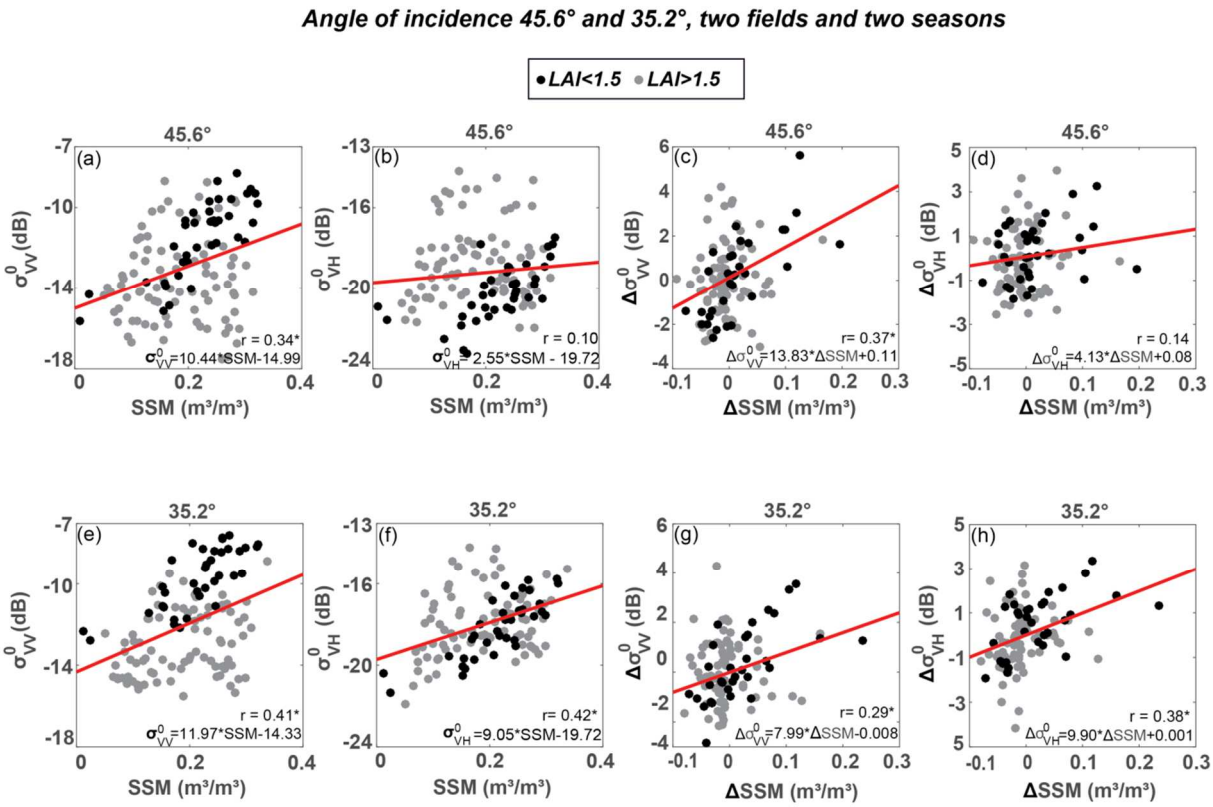

Fig. 4. Relationship between: (a, b) and (e, f) σ^0_{VV} and σ^0_{VH} and SSM, (c, d) and (g, h) $\Delta\sigma^0_{VV}$ and $\Delta\sigma^0_{VH}$ and ΔSSM at 45.6° and 35.2°. Data are shown separately for LAI<1.5 (black points) and LAI>1.5 (grey points). Statistical metrics are provided for the whole season. Correlations significant at 99% level are marked with a star ''.*

When data acquired over the entire season are considered, the relationships are obviously scattered (correlation coefficients r below 0.42; see Table T3). This is because the soil

contribution to the signal is progressively attenuated by the canopy when wheat grows. This results in a progressive decrease of the slope of the relationship between the backscattering coefficient (the backscattering difference between two acquisitions) and SSM (SSM differences) to reach almost no sensitivity to SSM change. Backscattering coefficients are on average better correlated with SSM at 35.2° than at 45.6° because of a stronger contribution of the soil at lower incidence angle. As expected also, VV polarization is more tightly related to SSM than VH at 45.6° as the contribution of the canopy is higher than at 35.2°. Slightly lower statistical metrics are obtained for the $\Delta\sigma^0/\Delta SSM$ relationships than for the direct relationships between σ^0 and SSM, in particular considering VV polarization at 35.2° (r=0.29 vs r=0.41) but the correlation coefficient is also significant at the 99% level at 45.6° (r=0.37) for VV polarization. Please note that this analysis may be biased because of the very specific growing conditions of Field 2 during the 2nd season including a strong horizontal extension of the adventices that may alter the relationship.

When wheat is not fully covering the soil (LAI<1.5 m²/m²), much better statistics are observed. In this case, significant correlations at the 99% level are obtained for all configurations (Table T3). Quite similar relationships σ^0/SSM are observed at 35.2° for VV and VH with r=0.76 and r=0.82, respectively while much significant differences in favor of VV are obtained at 45.6° as the vegetation contribution increases with the incidence angle. Likewise, at 35.2°, the slopes of the relations are similar ((17.4 and 16.7 dB/[m^3/m^3] for VH and VV respectively), while at 45.6°, higher sensitivity is observed for VV (21.5 dB/[m^3/m^3] compared to 12.7 dB/[m^3/m^3] for VH). For the $\Delta\sigma^0/\Delta$SSM, the best fitting is obtained for VV with r=0.70 and r=0.63 at 35.2° and 45.6°, respectively while the difference of metrics between VV and VH are more important with regards to σ^0/SSM. As expected, higher slopes

are observed at VV for both incidence angles with values of 14.1 dB/[m^3/m^3] and 24.4 dB/[m^3/m^3] at 35.2° and 45.6°, respectively.

These observations confirm the well known results: a higher sensitivity of the radar signal to soil contribution (and consequently soil moisture) for low incidence angles and VV polarization.

2.1.3. Polarization ratio, interferometric coherence and vegetation descriptors

In this section, the relationships between the interferometric coherence and PR, that both have been shown to be related to vegetation development, and AGB and VWC are analyzed. As NDVI can be obtained with similar spatio-temporal resolutions from Sentinel-2, the same relations are investigated with NDVI. Fig. 5 illustrates these relationships using the data of both fields and seasons, at 35.2° incidence angle. The points in black corresponds to the data acquired before AGB (or VWC) peak while data after the peak are plotted in grey. The same figure but with data acquired at 45.6° is provided as supplementary material (Fig. S6). Please note that an exponential fit is used for interferometric coherence while a polynomial fit is chosen between PR and VWC because both exhibit a “bell” shape.

The relationships between NDVI and AGB (Fig. 5a) and VWC (Fig. 5b) exhibit a strong dispersion and an hysteresis effect considering separately data acquired before and after the peak. While NDVI is mainly sensitive to the green leaf area index (GLAI), the relation between GLAI and VWC or AGB is not linear and depends on the plant structure. The hysteresis effect observed for the relation with AGB is simply related to the leaf senescence leading to a drastic drop of GLAI after the peak while AGB remain high. The relation saturates for low values of AGB (~ 0.3 kg/m^2). By contrast, the relationships are much better

when the polarization ratio and the interferometric coherence are considered. Considering the spearman rank correlation, the best relationships are obtained with VWC for both interferometric coherence and PR. For the PR, the relationships are good with both AGB and VWC on the entire crop cycle at 35.2with higher saturation values than with NDVI (AGB ~ 0.5 kg/m²). Unfortunately, the metrics seems not stable when the incidence angle is changing as poorer results are obtained at 45.6° (Fig. S6). Finally, good relationships are also obtained between interferometric coherence and AGB and VWC for both incidence angles with even higher saturation value (around 0.9 kg /m² for the relationship between ρ_{VV} and AGB at 35.2°). Our assumption is that coherence is less sensitive to the geometry of the canopy than the PR. Regarding the results above, the relationships between interferometric coherence at VV polarization and the PR on one hand and, on the other hand, AGB and VWC are potential candidates for the retrieval of SSM.

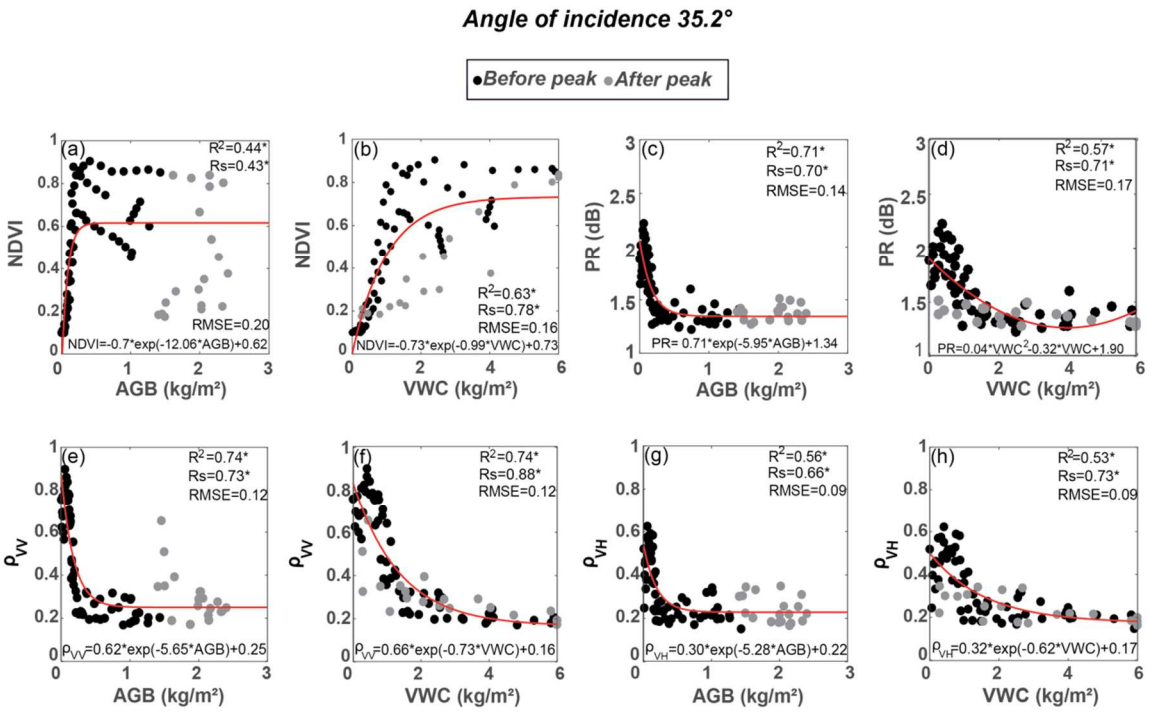

Fig. 5. Relationship between (a,b) NDVI and AGB and VWC; (c,d) PR and AGB and VWC; (e,f) ρ_{VV} and AGB and VWC; (g,h) ρ_{VH} and AGB and VWC at 35.2°. Black point corresponds to data acquired before the AGB (or VWC) peak while grey is for data after the peak. R² and Rs significant at the 99% are followed by a star (*).

2.2. Simulation results

Fig. 6 displays the time series of predicted and observed backscattering coefficients on both fields at 35.2° together with contributions from the soil attenuated by the canopy and from the canopy when using AGB as the vegetation descriptor. Fig. 7 is the same as Fig. 6 but at 45.6°. Table 5 summarizes the corresponding statistical metrics for calibration/ validation of the WCM. Several vegetation descriptors were tested among which LAI, Fc, NDVI, AGB and VWC. Fig. S7 and S8 in the supplementary material are the same as Fig.6 but using NDVI and VWC. By considering AGB (Fig. 6), the seasonal course of the backscattering coefficient is well reproduced for both incidences and both polarizations. The relative variations between the configurations (higher σ^0_{VV} than σ^0_{VH} and higher σ^0 at 35.2° than σ^0 at 45.6° for both polarizations) are also well reproduced demonstrating the proper calibration of the model. Obviously, the soil contribution that dominates the scattering mechanism during the first half of the season is progressively attenuated with the canopy development. As expected, (Fontanelli et al., 2013; Macelloni et al., 2001; Paloscia et al., 2014; Picard et al., 2003), soil attenuation is stronger for VV than for VH in response to the vertical stem extension. In March, when both soil and vegetation contributes, the agreement between observations and prediction deteriorates with regards to the rest of the cycle (RMSE=2.62 dB in March 2018 and 1.66 dB for the whole season for Field 1 at VV polarization and 35.2°).

During the second cycle, the agreement is also good even if a bias can be observed (up to 2.84 dB for Field 1 at VV polarization and 35.2°). For Field 2 during 2017-2018, the bias is to be attributed to the adverse growing conditions already highlighted. By contrast, the use of VWC and, to a lesser extent NDVI as vegetation descriptor (Fig. S7 and S8), suffer from several limitations during the second part of the season: (1) the observed decrease of the

backscattering coefficient from seeding to heading is poorly reproduced; (2) there is no second cycle and (3) the drop of backscattering coefficient at the end of the season occurred around 18 days earlier than observations. This is particularly prominent for VH polarization. As demonstrated by Picard et al. (2003) and Mattia et al. (2003), the backscattering mechanisms after heading is dominated by the volume scattering within the head layer partially shielding the stem and leaves below. Ulaby et al. (1986) suggested that an additional term needs to be added to the traditional three terms model (volume scattering from vegetation, soil attenuated and interaction soil-vegetation) to properly represent wheat backscattering after heading. This may explain why, for a simple model like the water cloud unable to separate between the contribution from the leaves, stems and heads, the use of AGB provided with the best predictions of the seasonal course of the backscattering, including the second increase occurring from the heading stage and the drop of σ^0 at the end of the season. Nevertheless, further investigations are needed to support this assumption by using a multi-layer radiative transfer model.

Table 5
Statistical metrics of the WCM calibration and validation (see text) at 45.6° and 35.2° of incidence angle and for VV and VH polarizations when using AGB as vegetation descriptor.

	Calibration				**Validation**							
	Field 1 & 2				Field 1				Field 2			
	45,6°		35,2°		45,6°		35,2°		45,6°		35,2°	
	VV	VH	VV	VH	VV	VH	VV	VH	VV	VH	VV	VH
r	0.73	0.47	0.76	0.24	0.72	0.46	0.73	0.61	0.56	0.52	0.68	0.43
RMSE	1.54	1.66	1.44	1.92	1.5	1.89	1.66	1.74	2.02	2.52	1.58	1.98
Bias	-0.17	0.25	-0.31	0.27	-0.39	0.02	-0.03	0.76	-0.03	0.54	0.08	0.32

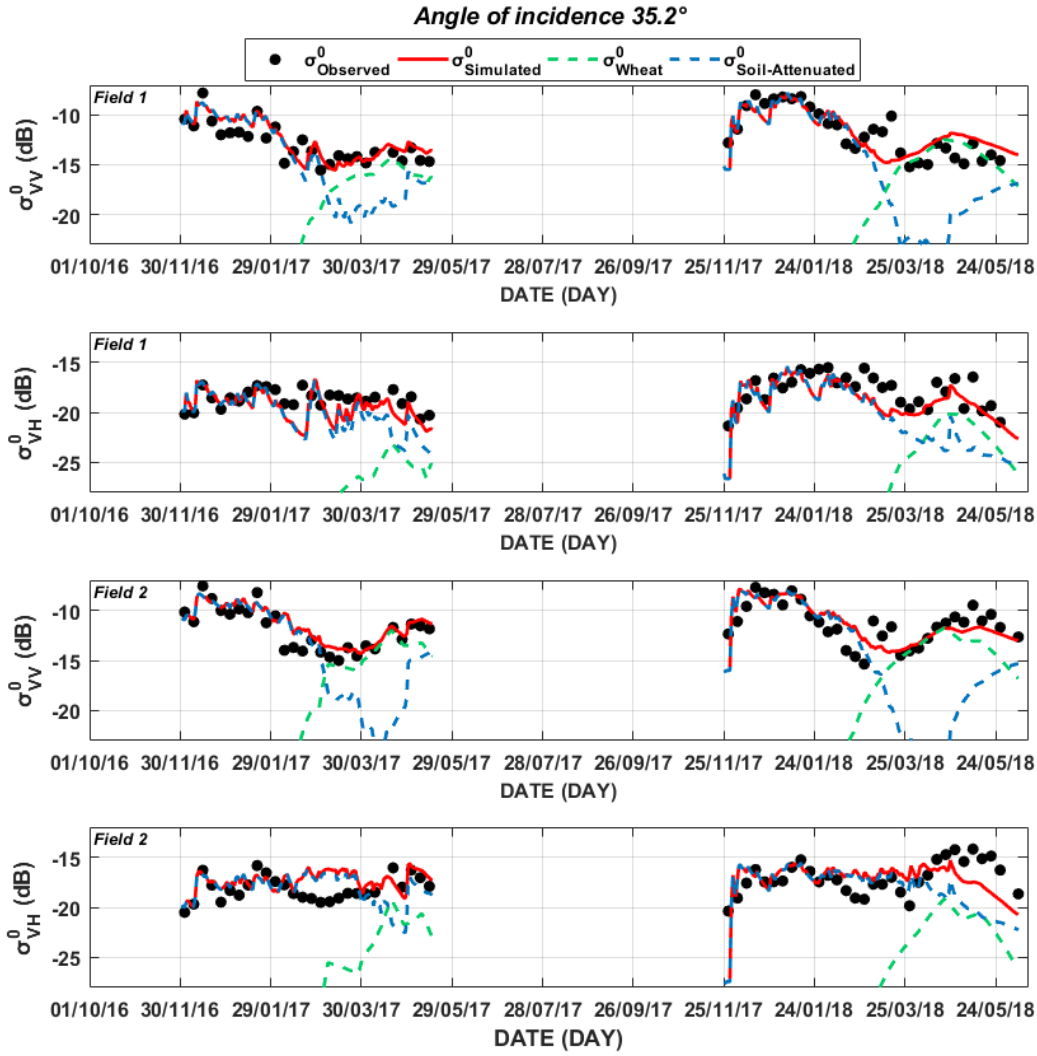

684

685 *Fig. 6. Time series of the different contributions simulated using the WCM and AGB as vegetation descriptor*
686 *fitting the observations at VV and VH polarizations over Field 1 and Field 2 and for both seasons (2016-2017 and*
687 *2017-2018) at 35.2° of incidence angle.*

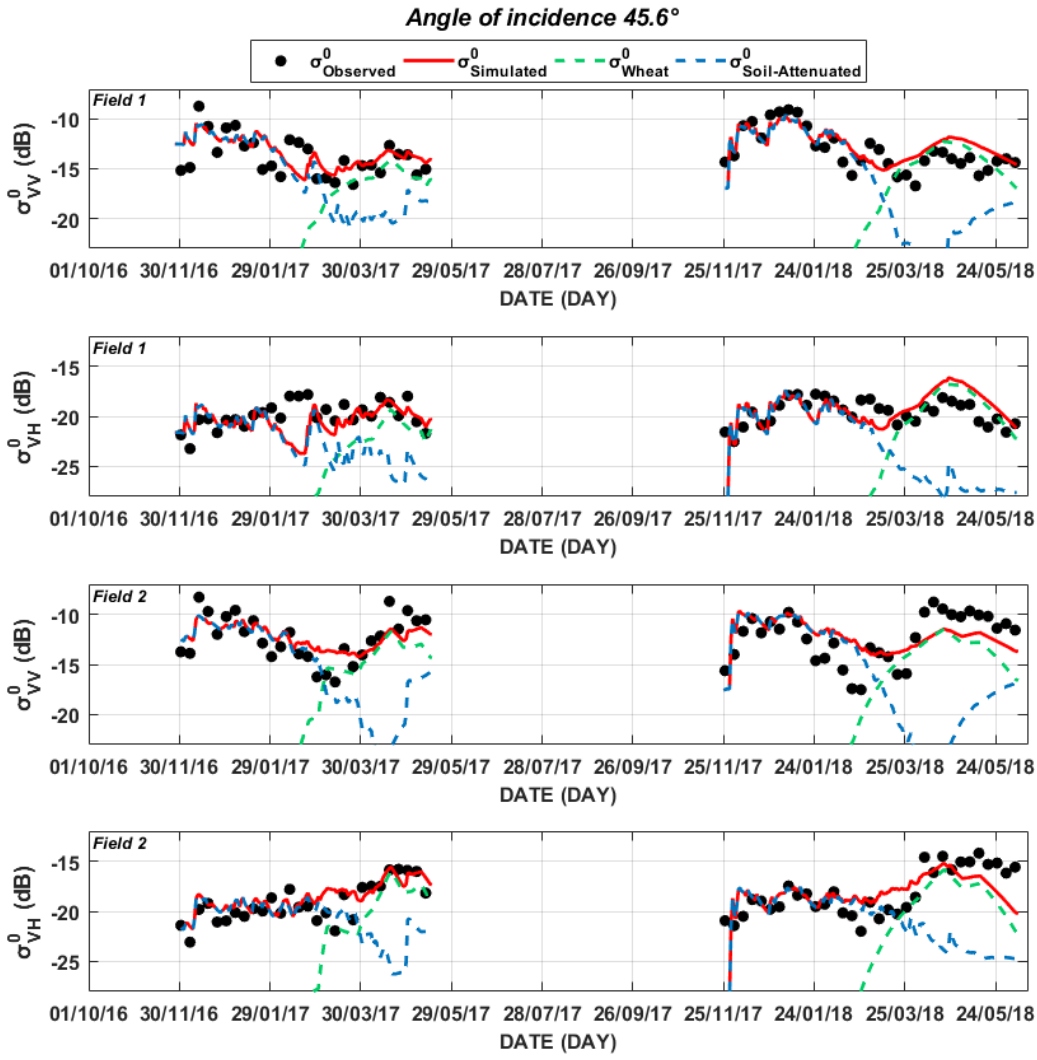

Fig. 7. Time series of the different contributions simulated using the WCM and AGB as vegetation descriptor fitting the observations at VV and VH polarizations over Field 1 and Field 2 and for both seasons (2016-2017 and 2017-2018) at 45.6° of incidence angle.

2.3. Surface soil moisture retrieval

The focus of this section is on the retrieval of the SSM on wheat crops during the whole growing season using Sentinel-1 information only. The results of the two proposed approaches, based on the interferometric coherence and on the polarization ratio, are compared to three extensively used methods and discussed. The good relationship obtained between either the coherence ρ_{VV} or PR, and AGB or VWC, are used (Fig. 5e). Table 6 summarizes the statistical metrics for the whole crop season.

Table 6

Statistical metrics of the surface soil moisture estimation using the seven methods (see text) for the calibration sites. Bold correlation coefficients are significant at the 99% level.

		Field 1				Field 2				Field 3			
		45.6°		35.2°		45.6°		35.2°		45.6°		35.2°	
		VV	VH	VV	VH	VV	VH	VV	VH	f	VH	VV	VH
$WCM_{\rho-AGB}$	r	**0.6**	**0.34**	**0.82**	**0.73**	0.01	0.13	0.29	0.3	**0.71**	0.4	**0.8**	0.21
	RMSE	0.08	0.09	0.05	0.06	0.13	0.11	0.09	0.08	0.04	0.09	0.04	0.08
	Bias	-0.03	-0.06	0	-0.03	0	-0.02	0.02	-0.03	0.03	-0.07	0.01	0.06
	slope	0.85	0.27	0.93	0.61	0.02	-0.17	0.3	0.28	0.69	0.59	1.05	0.19
$WCM_{\rho-VWC}$	r	**0.62**	**0.4**	**0.59**	**0.58**	0.18	0.31	0.1	-0.1	**0.66**	**0.47**	**0.69**	**0.5**
	RMSE	0.08	0.1	0.08	0.08	0.16	0.18	0.11	0.14	0.06	0.09	0.05	0.08
	Bias	0.02	-0.01	-0.02	-0.03	0.01	0.03	-0.01	0.03	0.05	-0.07	0.02	-0.07
	Slope	0.91	0.58	0.83	0.72	0.39	-0.61	0.16	-0.33	0.72	0.73	0.9	0.51
WCM_{PR-AGB}	r	0.26	**0.39**	**0.61**	**0.61**	0.04	-0.42	0.01	0.18	**0.76**	0.37	**0.68**	**0.47**
	RMSE	0.22	0.08	0.12	0.07	0.23	0.19	0.2	0.14	0.05	0.08	0.08	0.08
	Bias	-0.15	-0.04	0.02	-0.03	-0.16	-0.03	-0.01	0	0.04	0.05	0.05	-0.05
	Slope	0.57	0.35	1.3	0.71	0.13	-0.73	0.02	-0.23	0.8	0.57	1.09	0.57
WCM_{PR-VWC}	r	**0,55**	0,32	**0,67**	**0,56**	-0.19	-0.38	0.06	-0.15	**0,61**	**0,47**	**0,68**	**0,59**
	RMSE	0,09	0,12	0,06	0,1	0.17	0.21	0.11	0.18	0,08	0,08	0,06	0,09
	Bias	0,02	0,01	-0,01	0	0.01	-0.03	0	0	0,06	0	0,02	-0,02
	Slope	0,88	0,56	0,7	0,9	-0.46	-1.1	0.10	-0.39	0,76	1,04	0,95	1,18
WCM_{NDVI}	r	**0.57**	0.16	**0.65**	**0.53**	-0.2	-0.45	0.21	0.29	**0.57**	0.35	**0.7**	**0.53**
	RMSE	0.09	0.13	0.08	0.09	0.2	0.23	0.12	0.18	0.07	0.09	0.05	0.1
	Bias	0.01	-0.03	-0.01	-0.04	0.01	0	-0.01	0.02	0.06	0.05	0.03	-0.06
	slope	0.89	0.26	0.89	0.68	0.51	-1.15	0.37	-0.63	0.62	0.6	0.8	0.64
σ^0	r	**0.63**	0.28	**0.67**	**0.66**	-0.11	0.3	0	0.03	**0.6**	0.23	**0.61**	0.42
	RMSE	0.07	0.07	0.07	0.07	0.07	0.08	0.07	0.07	0.08	0.07	0.08	0.08
	Bias	-0.04	-0.02	-0.04	-0.04	0.02	0.05	0.02	0.01	-0.07	-0.06	-0.06	-0.06
	slope	0.11	-0.01	0.19	0.25	-0.02	0.01	0	0.01	0.12	-0.01	0.25	0.19
$\Delta\sigma^0$	r	0.29	0.21	**0.38**	**0.35**	**0.43**	0.09	0.21	0.42	**0.71**	**0.62**	**0.65**	0.15
	RMSE	0.04	0.04	0.04	0.04	0.05	0.05	0.05	0.05	0.07	0.07	0.07	0.06
	Bias	0	0.07	0	0	0	0	0	0	0.06	0.05	0.06	0.04
	Slope	0.08	0.02	0.13	0.17	0.11	0.01	0.06	0.17	0.31	0.24	0.15	0.02

All the methods are able to retrieve SSM reasonably well at 35.2° using VV backscattering coefficients on Field 1 and Field 3 with r above 0.60 apart for the empirical approach based on $\Delta\sigma^0$ in Field 1 (r=0.38 at 35°2 and VV polarization). By contrast, SSM for most of the methods and, in particular for those based on the WCM, performed poorly on Field 2. For

information, for the WCM based approaches, the retrieval on Field 2 has also been tested by calibrating the WCM on the second season or by using the calibrated coefficient of Field 1. In both cases, poor results were obtained. This is attributed to very specific growing conditions that severely affected the wheat development as already discussed (see pictures Fig. S1 and Fig.S2 of the supplementary materials). Indeed, if data from the beginning of the season (LAI < 1.5 m^2/m^2) only are considered, results are similar to those obtained on Field 1 at both 45.6° and 35.2° meaning that the main issue is related to the development of the vegetation in this field. This illustrates that the performance of the model based approaches could drop drastically when growth conditions diverge significantly, in terms of vegetation structure in particular, from the conditions on which the model was calibrated. Interestingly enough, the empirical technique based on $\Delta\sigma^0$ performed very well on Field 3 (r=0.71) and to a lesser extent on Field 2 (r=0.43). It is the best from all the evaluated methods on Field 2. In addition, it provided with the lowest RMSE (RMSE < 0.05 m^3/m^3) on Field 1 & 2 but 0.07 m^3/m^3 on Field 3. The best results are obtained on Field 1 by the new WCM based approach using the relation between the interferometric coherence and AGB (r=0.82, RMSE=0.05 m^3/m^3 and no bias for VV at 35.2°). For illustration purpose, Fig. 8 displays the scatter plots between the observed and retrieved SSM using the latter method from sowing to harvest at 35.2°: (a) and (b) are for Field 1 at VV and VH, respectively; (c) and (d) are for Field 2 and (e) and (f) for Field 3. Metrics are obviously worse at 45.6° because of a stronger contribution of the canopy and for VH polarization for all considered methods.

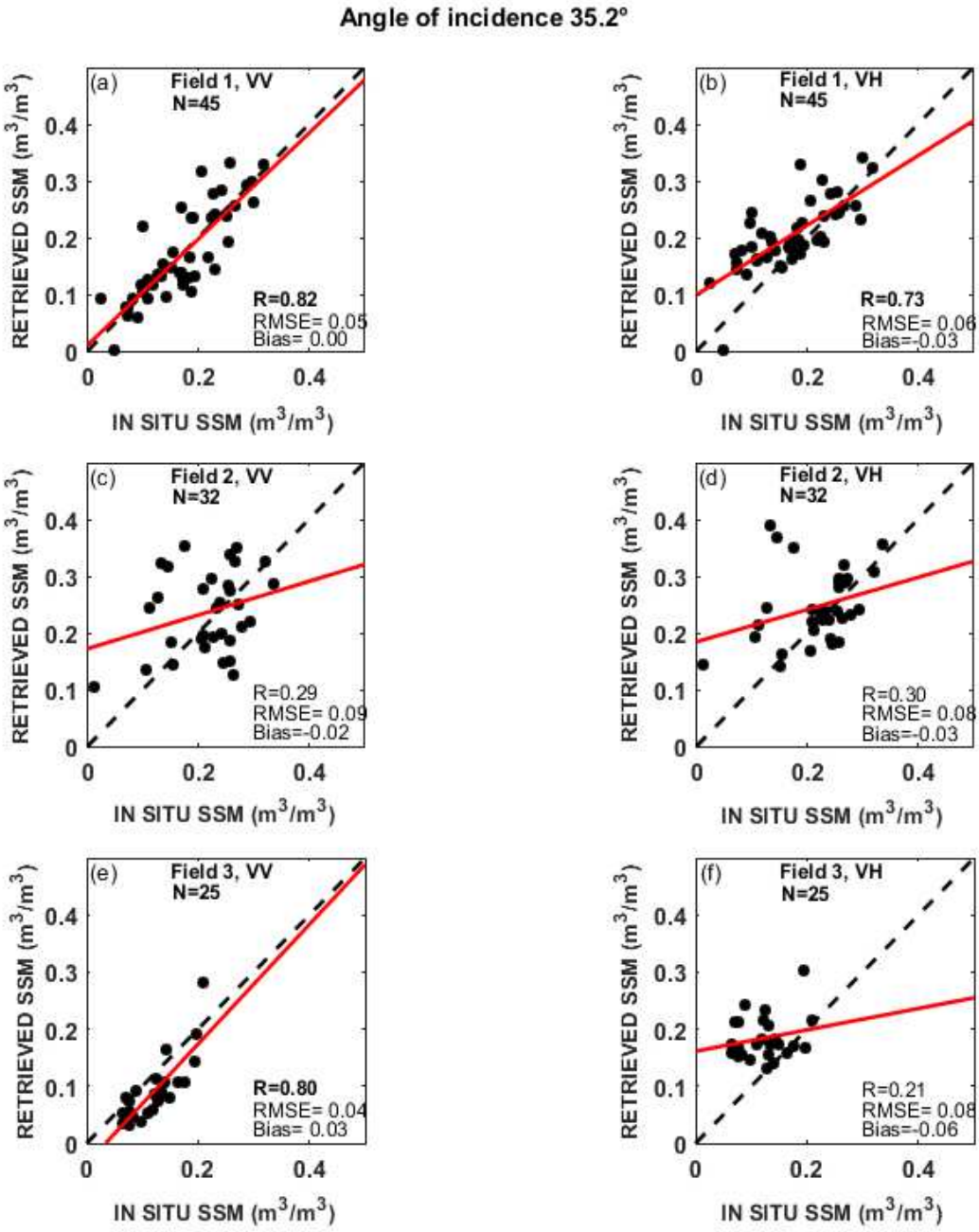

727

728 *Fig. 8. Retrieved SSM versus in situ measurements at VV and VH polarizations at 35.2° of incidence angle for the*
729 *calibration sites: (a,b) Field 1, (c,d) Field 2 and (e,f) Field 3. Bold correlation coefficients are significant at the*
730 *99% level.*

731

732 In order to evaluate the genericity of all methods, they have been implemented on the
733 validation database using the calibration carried out on Field 1 and Field 2 during the first
734 crop season. Table 7 displays the statistical metrics for the seven methods on the validation

735 database mixing rainfed and irrigated fields. All methods performed reasonably well at VV
736 polarization including the simplest approaches based on σ^0 and $\Delta\sigma^0$ with correlation
737 coefficients always significant at the 99% level apart from the $\Delta\sigma^0$ method on the "Sidi
738 Rahal" site (rainfed). Results are slightly worse but remain close to the ones obtained on the
739 site where the methods were calibrated for the three other approaches (WCM_{NDVI}, σ^0 and
740 $\Delta\sigma^0$). In addition, the lower correlation on "Sidi Rahal" and on the Tunisian plots could also
741 be due to the slightly higher incidence angle of the Sentinel-1 data acquired on these two
742 last site (40° versus 35.2° for the sites where the method has been calibrated). By contrast,
743 overall performances are worse for the empirical approaches but they appear more stable
744 from one site to another, in particular for the σ^0 based method as demonstrated by the small
745 changes of correlation coefficient ranging from 0.60 to 0.62 and of RMSE (0.07 m^3/m^3).
746 Despite the moderate loss of performance from the fields of "Domaine Rafi" to the
747 validation sites, the method based on the $\rho - AGB$ relationships provided with the best
748 results on the validation database with systematically higher correlation coefficients, lower
749 RMSE and biases remaining low with a maximum value of 0.03 m^3/m^3 for VV polarization
750 and an average bias of 0.01 m^3/m^3 on the entire database. For illustration purpose, Fig. 9
751 displays the scatter plot in the rainfed field, Morocco (a and b) and in the Kairouan plain,
752 Tunisia (c and d) for the latter approach. Fig. 9e and f shows the scatterplots for the whole
753 database including Field 1 and Field 3.

754

755 *Table 7*
756 *Statistical metrics of the surface soil moisture estimation using the seven methods (see text) on the validation*
757 *database. Bold correlation coefficients are significant at the 99% level.*

Sidi Rahal	Kairouan
40°	40°

		VV	VH	VV	VH
$WCM_{\rho-AGB}$	r	**0.7**	**0.61**	**0.75**	**0.54**
	RMSE	0.08	0.08	0.06	0.06
	Bias	0.03	0.03	0.01	0.04
	Slope	0.76	0.52	0.64	0.47
$WCM_{\rho-VWC}$	r	**0.68**	**0.63**	**0.65**	**0.42**
	RMSE	0.11	0.08	0.07	0.1
	Bias	0.08	0.02	0.01	-0.05
	Slope	0.7	0.58	0.62	0.38
WCM_{PR-AGB}	r	**0.59**	**0.52**	**0.61**	**0.39**
	RMSE	0.13	0.11	0.08	0.09
	Bias	0.09	0.05	0.02	-0.03
	Slope	0.71	0.54	0.7	0.39
WCM_{PR-VWC}	r	**0,69**	**0,5**	**0,64**	**0,37**
	RMSE	0,1	0,11	0,07	0,1
	Bias	0,07	0,04	0,01	-0,04
	Slope	0,73	0,56	0,56	0,35
WCM_{NDVI}	r	**0.69**	**0.56**	**0.61**	**0.39**
	RMSE	0.1	0.1	0.07	0.1
	Bias	0.07	0.03	0.02	-0.04
	Slope	0.71	0.62	0.62	0.39
σ^0	r	**0.6**	**0.59**	**0.62**	**0.42**
	RMSE	0.07	0.07	0.07	0.07
	Bias	0.02	0.02	-0.01	0
	slope	0.5	0.4	0.12	0.15
$\Delta\sigma^0$	r	0.24	-0.36	**0.24**	**0.24**
	RMSE	0.18	0.24	0.11	0.11
	Bias	0.11	0.15	-0.05	-0.06
	Slope	-0.24	-0.51	0.28	0.25

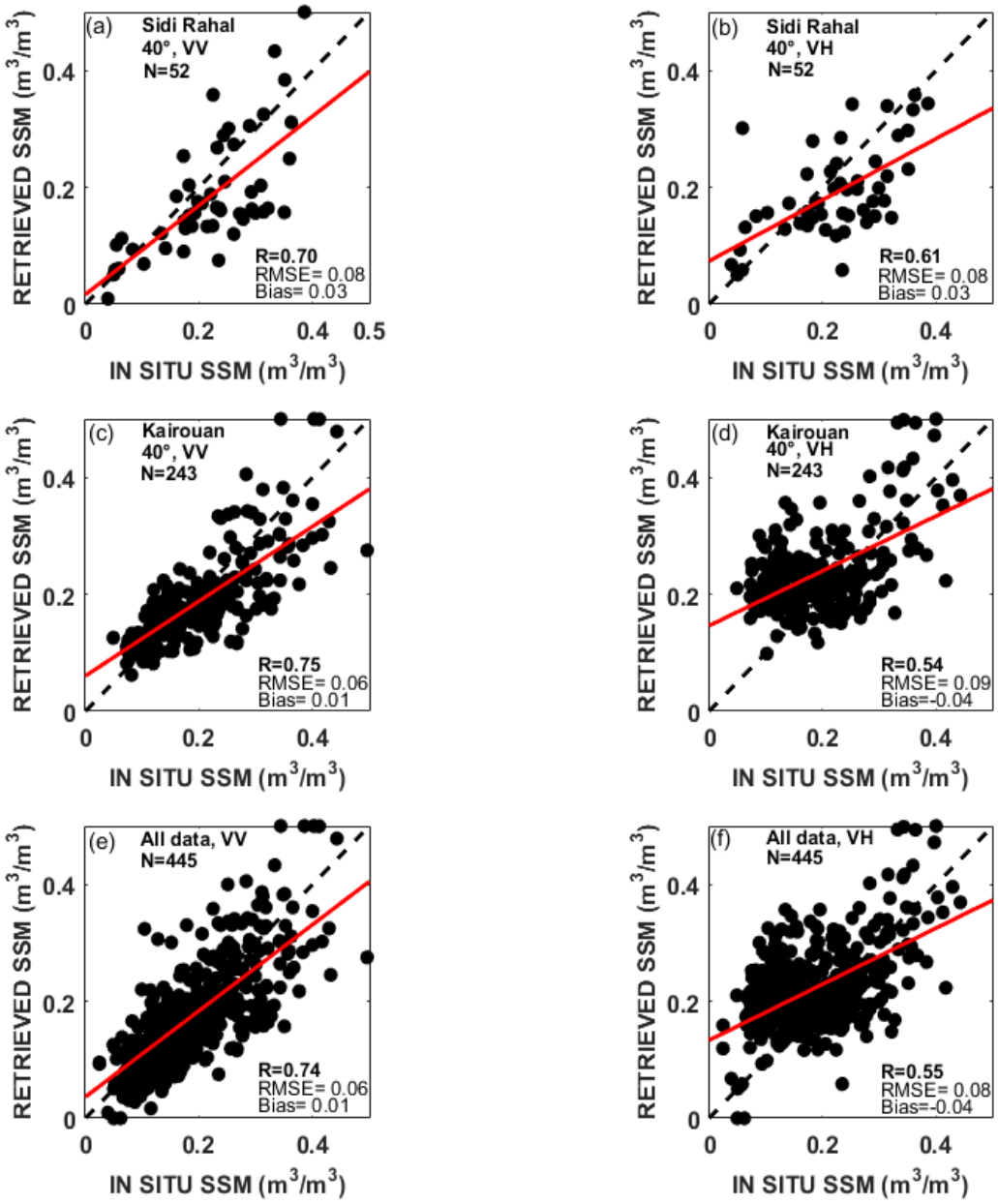

761

762 *Fig. 9. Retrieved SSM versus in situ measurements at VV and VH polarizations over the validation sites for the*
763 *coherence based approach:(a,b) Sidi Rahal; (c,d) 18 plots of Kairouan plain (~40°); (e,f) All data (all fields and all*
764 *orbits). Bold correlation coefficients are significant at the 99% level.*

765

766 In order to evaluate the potential loss of performance associated to vegetation growth, the
767 correlation coefficients of the seven methods are plotted as a function of AGB in Fig. 10
768 using data of Field 1 and Field 3 because *in situ* measurements of AGB were available on
769 these fields. Field 2 was discarded because of the specific growing conditions already

discussed. The number of points ranges from 26 at the start of the crop season (AGB<=0.14 kg/m² corresponding to LAI<=1.5 m²/m²) to 70 when all vegetation conditions are considered (AGB<=2.50 kg/m²). When soil contribution is dominating the signal at the beginning of the season, performances of the seven retrieval methods are of the same order with correlation coefficients above 0.70 for VV polarization. When soil is progressively shielded by the canopy as vegetation growths, a drop of r is observed for most of the methods as expected and r increases again afterwards or remains almost constant. This is because most of the observations corresponding to AGB values above 1.5 kg/m² are acquired during the senescence period when wheat dries out and the soil contribution to the backscattering become significant again (cf simulation results). The lower drop is observed for the $WCM_{\rho-AGB}$ as r goes from 0.80 to 0.78 (about 2.5%). By contrast, r decreases of more than 18% for all the others WCM based approaches (WCM_{NDVI}, WCM_{PR-AGB}, WCM_{PR-VWC} and $WCM_{\rho-VWC}$). Interestingly enough, despite the empirical approach based on σ^0 provides with slightly lower performances than the WCM based techniques at the start of the season, it shows a good stability as the drop of r associated to vegetation development is low (around 13%). The lower performances of the $\Delta\sigma^0(\Delta SSM)$ approach are in close agreement with the paper of El Hajj et al. (2019) who show that it offered poor performance at C-Band for NDVI greater than 0.7.

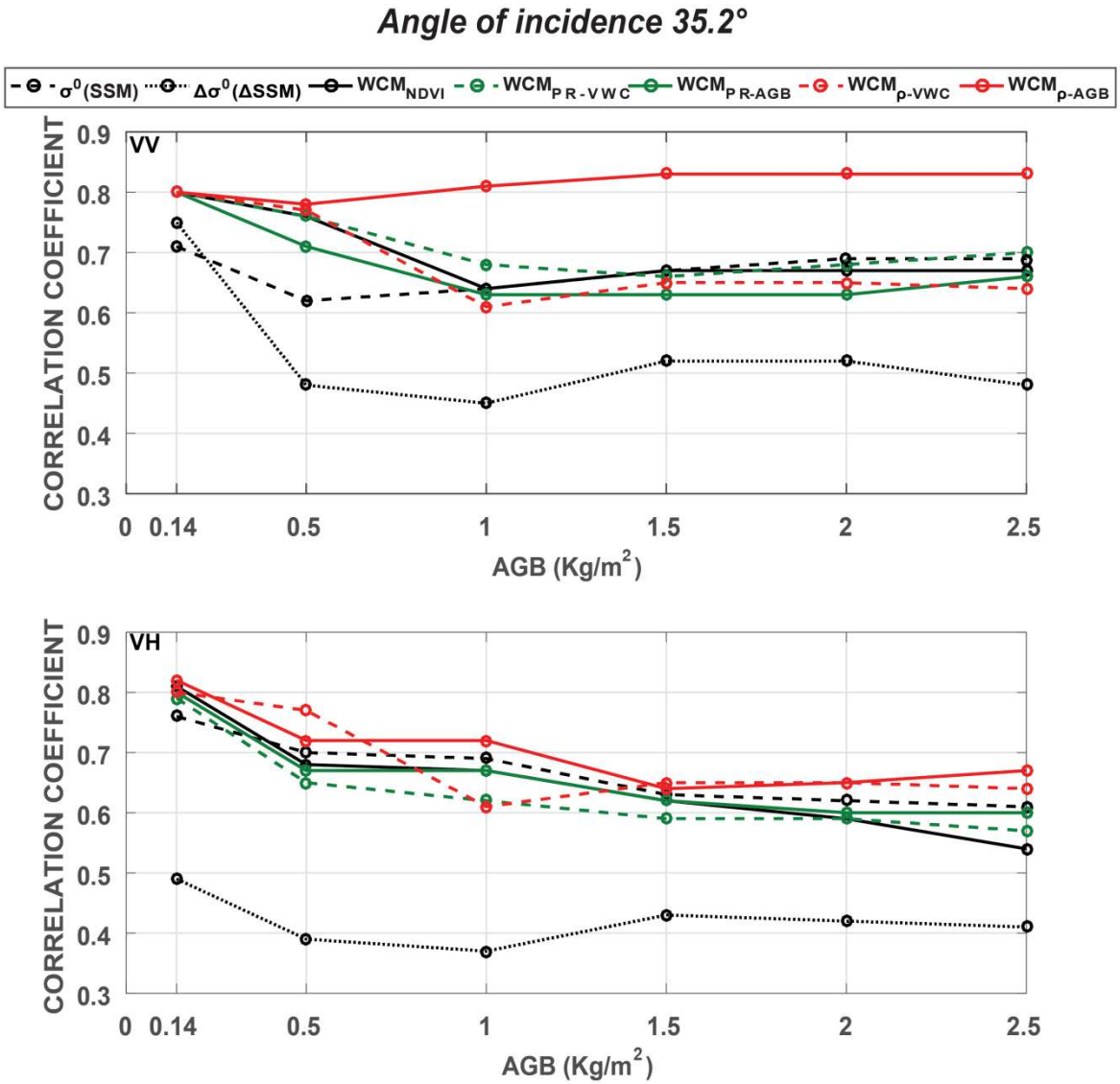

789

790 *Fig. 10. Correlation coefficient between the observed and the retrieved SSM as a function of AGB using data of*
791 *Field 1 and Field 3 at 35.2° and VV and VH polarizations for the seven methods: σ^0(SSM), $\Delta\sigma^0$ (ΔSSM), WCM_{NDVI},*
792 *WCM_{PR-VWC}, WCM_{PR-AGB}, $WCM_{\rho-VWC}$, $WCM_{\rho-AGB}$. All the correlations are significant at the 99% level.*

793 Finally, the $WCM_{\rho-AGB}$ was implemented to map SSM over an irrigated perimeter located 40
794 km east of Marrakech name R3 (Duchemin et al., 2006) for illustration purpose. The
795 perimeter is dominated by wheat even if some vegetables and trees are also cropped. Fig. 11
796 displays maps of SSM for two contrasted dates: (1) 15/01/2017 during the crop season when
797 wheat is irrigated, and (2) 20/06/2017 when all wheat fields have been harvested. Tree fields
798 are masked thanks to a land use map from the 2012-2013 crop season (Diarra et al., 2017)
799 and an aerial picture acquired in 2019 from Google map. In January, most of the fields are

wet with soil moisture values reaching 0.4 m^3/m^3 while drier conditions are encountered in June. An interesting feature is the high variability of hydric conditions from one field to another during January in relation to irrigation distribution and sowing date. A complete water turn takes about 15 days to irrigate all the fields introducing also a large diversity in terms of hydric condition. The SSM map of January depicts well this variability. The large oblique patch located west of the images exhibiting dry conditions on both date corresponds to bare soil that are never cropped.

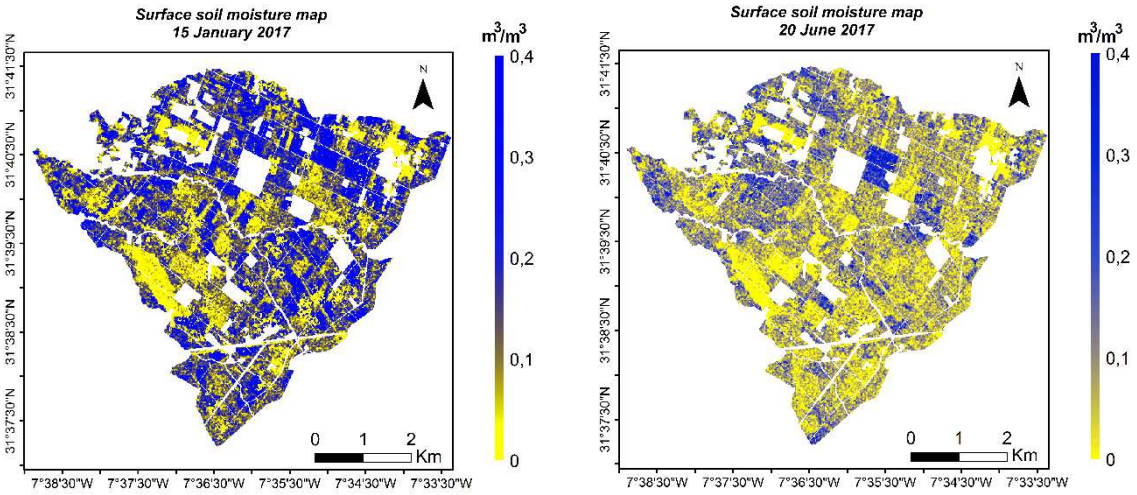

Fig. 11. Surface soil moisture maps over an irrigated perimeter located 40 km east of Marrakech named R3 for two different SSM conditions : wet condition (15 January 2017) and dry condition (20 June 2017).

Summary and conclusion

The objective of this work was to develop and evaluate a new approach for surface soil moisture (SSM) retrieval over wheat crops based on Sentinel-1 data. The goal was to rely on Sentinel-1 only, without any additional ancillary data. This work is based on a large *in situ* database from several irrigated and rainfed wheat in Morocco and Tunisia. A comprehensive study of wheat C-band radar response was conducted. The time series of the backscattering coefficient and the interferometric coherence derived from C-band Sentinel-1 are analyzed and physically interpreted. The analysis showed that the backscattering coefficient is obviously sensitive to the surface soil moisture changes, at least during the first stage of wheat growth, while the interferometric coherence and PR are more affected by the wheat crop growth. The good relationships obtained between PR/interferometric coherence, on one hand and, on the other hand, AGB/VWC were selected as potential candidates for the retrieval of SSM. The WCM coupled to Oh model was calibrated at VV and VH polarization and for two angles of incidence (45.6° and 35.2°). Several parameters were tested as descriptors of wheat development but observed backscattering coefficients after the heading stage was better reproduced using the AGB. The model showed to reasonably reproduce the observed seasonal course of the backscattering coefficient if the empirical coefficients of the WCM were calibrated separately for VV and VH. The calibrated model was used in an inversion process for the SSM. The four methods are named $\mathrm{WCM_{PR-VWC}}$, $\mathrm{WCM_{PR-AGB}}$, $\mathrm{WCM_{\rho-VWC}}$ and $\mathrm{WCM_{\rho-AGB}}$. They are compared to three more classical methods for SSM retrieval composed of two empirical approaches (linear relationships $\sigma^0 - SSM$ and $\Delta\sigma^0 - \Delta SSM$) and one based on the water-cloud model but with NDVI as the vegetation descriptor ($\mathrm{WCM_{NDVI}}$). Please note that the new WCM based

approaches require additional measurements of the vegetation characteristics to develop the relationships between PR/ ρ - AGB/VWC adding three parameters to be fitted with regards to $\mathrm{WCM_{NDVI}}$, $\sigma^0(SSM)$ and $\Delta\sigma^0(\Delta SSM)$ methods. The main results can be summarized as follows:

- All methods performed reasonably well at VV polarization with better results for the WCM-based when compared to the empirical ones (σ^0 and $\Delta\sigma^0$).
- Despite a moderate variability of the statistical metrics when going from one site to another, the new method based on the relationship between the interferometric coherence and the AGB provided with the best results with a correlation coefficient r of 0.74 and a small bias of 0.01 m^3/m^3.
- By contrast, overall performances were worse for the empirical approaches but they were more stable from one site to another, in particular for the σ^0 based method.

The proposed new approaches taking advantage of two complementary and relatively independent information derived from Sentinel-1 data made it possible to get away from dependence on optical data that are restricted by weather and illumination conditions. They are valid for wheat crops (as the relationships between the interferometric coherence/PR and vegetation characteristics were established for wheat) during the period from seeding after all soil tillering action to harvest only meaning three conditions must be satisfied: (1) soil roughness parameter h_{rms} remains within the range from 0.7 to 1.5 cm; (2) there is no drastic change of soil roughness during the crop season. Stated differently, no soil tillering is done from seeding to harvest; ; (3) the sensitivity of interferometric coherence to soil moisture change is of a 2nd order with regards to AGB and VWC changes; (4) they reflect the sensitivity of the radar signal to the vegetation geometrical structure, which can induce

significant errors if it is not well taken into account (explaining low results over the second test field).

The limited loss of performances on the validation database of the coherence based technique points out that it could be applied with a reasonable accuracy on sites outside of the area where it has been developed. This question of the genericity of the retrieval approach is fundamental. Very similar wheat varieties are sown in the south Mediterranean region meaning that the canopy structure are similar. Likewise, the fact that the phenological stages are very close as all the fields in our database are located in the South Mediterranean region lead to similar development of the plants. A strong change of structure would probably impact negatively the results. This means that the method would not be valid for different crop and in particular row crops such as sunflower. Even for wheat field, specific conditions such as the development of adventices with a different structure of wheat or stems laid down by the wind degrade the performance of the approach as demonstrated by the poor results obtained on Field 2. Further validation is thus required.

Further investigations will focused on the combination of C and L-band data within the frame of the numerous L-band mission in preparation (ROSE-L, NISAR) or already into orbit (ALOS-2, SAOCOM) for the joint retrieval of SSM and vegetation biomass, potentially separating its stems and heads components. Another aspect of our work in progress deals also with irrigated area mapping from which high spatio-temporal resolution SSM images could benefit (Malbéteau et al., 2018) together with irrigation retrieval at the plot scale.

Acknowledgements

878 This work was conducted within the frame of the International Joint Laboratory TREMA
879 (https://www.lmi-trema.ma/). The authors wish to thank the projects: Rise-H2020-ACCWA
880 (grant agreement no: 823965) and ERANETMED03-62 CHAAMS for partly funding the
881 experiments. Nadia Ouaadi was awarded mobility research training grants from PHC
882 TBK/18/61 and from the MISTRALS/SICMED program. We would like to thank also the
883 Moroccan CNRST for awarding a PhD scholarship to Nadia Ouaadi. ESA is acknowledged for
884 providing free products of Sentinel-1 and the authors are grateful to Theia for producing and
885 distributing Sentinel-2 images corrected from atmospheric effects. Finally, we would like to
886 acknowledge Dr. Omar Rafi, the owner of the “Domaine Rafi”, for his long-lasting support to
887 our research activities.

888

References

Ait Hssaine, B., Merlin, O., Rafi, Z., Ezzahar, J., Jarlan, L., Khabba, S., Er-raki, S., 2018. Calibrating an evapotranspiration model using radiometric surface temperature , vegetation cover fraction and near-surface soil moisture data. Agric. For. Meteorol. 257, 104–115. https://doi.org/10.1016/j.agrformet.2018.02.033

Allen, R.G., Pereira, L.S., RAES, D., SMITH, M., 1998. Crop Evapotranspiration—Guidelines for Computing Crop Water Requirements, Irrigation and Drain, Paper No. 56. FAO, Rome, Italy,.

Amazirh, A., Merlin, O., Er-raki, S., Gao, Q., Rivalland, V., Malbeteau, Y., Khabba, S., José, M., 2018. surface soil moisture at high spatio-temporal resolution from a synergy between Sentinel-1 radar and Landsat thermal data : A study case over bare soil. Remote Sens. Environ. 211, 321–337. https://doi.org/10.1016/j.rse.2018.04.013

Attema, E.P.W., Ulaby, F.T., 1978. Vegetation modeled as a water cloud. Radio Sci. 13, 357–364. https://doi.org/https://doi.org/10.1029/RS013i002p00357

Baghdadi, N., Cerdan, O., Zribi, M., Auzet, V., Darboux, F., El Hajj, M., Kheir, R.B., 2008. Operational performance of current synthetic aperture radar sensors in mapping soil surface characteristics in agricultural environments: Application to hydrological and erosion modelling. Hydrol. Process. https://doi.org/10.1002/hyp.6609

Baghdadi, N., El Hajj, M., Zribi, M., Bousbih, S., 2017. Calibration of the Water Cloud Model at C-Band for Winter Crop Fields and Grasslands. Remote Sens. 969, 1–13. https://doi.org/10.3390/rs9090969

Bai, X., He, B., Li, X., Zeng, J., Wang, X., Wang, Z., Zeng, Y., Su, Z., 2017. First assessment of Sentinel-1A data for surface soil moisture estimations using a coupled water cloud model and advanced integral equation model over the Tibetan Plateau. Remote Sens. 9, 1–20. https://doi.org/10.3390/rs9070714

Balenzano, A., Mattia, F., Member, S., Satalino, G., Davidson, M.W.J., 2011. Dense Temporal Series of C- and L-band SAR Data for Soil Moisture Retrieval Over Agricultural Crops. IEEE J. Sel. Top. Appl. EARTH Obs. Remote Sens. 4, 439–450. https://doi.org/10.1109/JSTARS.2010.2052916

Bamler, R., Hartl, P., 1998. Synthetic aperture radar interferometry. Inverse Probl. 14, 1–54. https://doi.org/10.1088/0266-5611/14/4/001

Bertuzzi, P., Chànzy, A., Vidal-Madjar, D., Autret, M., 1992. The use of a microwave backscatter model for retrieving soil moisture over bare soil. Int. J. Remote Sens. https://doi.org/10.1080/01431169208904070

Bindlish, R., Barros, A.P., 2001. Parameterization of vegetation backscatter in radar-based, soil moisture estimation. Remote Sens. Environ. 76, 130–137. https://doi.org/10.1016/S0034-4257(00)00200-5

Bindlish, R., Barros, A.P., 2000. Multifrequency soil moisture inversion from SAR measurements with the use of IEM. Remote Sens. Environ. https://doi.org/10.1016/S0034-4257(99)00065-6

Blaes, X., Defourny, P., 2003. Retrieving crop parameters based on tandem ERS 1 / 2 interferometric coherence images. Remote Sens. Environ. 88, 374–385. https://doi.org/10.1016/j.rse.2003.08.008

Bousbih, S., Zribi, M., Lili-Chabaane, Z., Baghdadi, N., El Hajj, M., Gao, Q., Mougenot, B., 2017. Potential of sentinel-1 radar data for the assessment of soil and cereal cover parameters. Sensors (Switzerland) 17. https://doi.org/10.3390/s17112617

Bousbih, S., Zribi, M., Pelletier, C., Gorrab, A., Lili-Chabaane, Z., Baghdadi, N., Aissa, N. Ben, Mougenot, B., 2019. Soil texture estimation using radar and optical data from Sentinel-1 and Sentinel-2. Remote Sens. 11. https://doi.org/10.3390/rs11131520

Brisco, B., Brown, R., Koehler, J.A., Sofko, G.J., Mckibben, M.J., 1990. The Diurnal Pattern of Microwave Backscattering by Wheat. Remote Sens. Environ. 34, 37–47. https://doi.org/10.1016/0034-4257(90)90082-W

Brown, S.C.M., Quegan, S., Morrison, K., Bennett, J.C., Cookmartin, G., 2003. High-resolution measurements of scattering in wheat canopies - Implications for crop parameter retrieval. IEEE Trans. Geosci. Remote Sens. 41, 1602–1610. https://doi.org/10.1109/TGRS.2003.814132

CNES, 2018. The ORFEO Tool Box Software Guide.

Dabrowska-Zielinska, K., Musial, J., Malinska, A., Budzynska, M., Gurdak, R., Kiryla, W., Bartold, M., Grzybowski, P., 2018. Soil moisture in the Biebrza Wetlands retrieved from Sentinel-1 imagery. Remote Sens. https://doi.org/10.3390/rs10121979

De Zan, F., Parizzi, A., Prats-Iraola, P., López-dekker, P., 2014. A SAR Interferometric Model for Soil Moisture. IEEE Trans. Geosci. Remote Sens. 52, 418–425.

Diarra, A., Jarlan, L., Er-Raki, S., Le Page, M., Aouade, G., Tavernier, A., Boulet, G., Ezzahar, J., Merlin, O., Khabba, S., 2017. Performance of the two-source energy budget (TSEB) model for the monitoring of evapotranspiration over irrigated annual crops in North Africa. Agric. Water Manag. 193. https://doi.org/10.1016/j.agwat.2017.08.007

Dobson, M.C., Ulabz, F.T., 1981. Microwave Backscatter Dependence on Surface Roughness , Soil Moisture , and Soil Texture : Part Ill-Soil Tension. IEEE Trans. Geosci. Remote Sens. GE-19, 51–61. https://doi.org/10.1109/TGRS.1981.350328

Duchemin, B., Hadria, R., Erraki, S., Boulet, G., 2006. Monitoring wheat phenology and irrigation in Central Morocco : On the use of relationships between evapotranspiration , crops coefficients , leaf area index and remotely-sensed vegetation indices 79, 1–27. https://doi.org/10.1016/j.agwat.2005.02.013

El Hajj, M., Baghdadi, N., Bazzi, H., Zribi, M., 2019. Penetration Analysis of SAR Signals in the C and L Bands for Wheat, Maize, and Grasslands. Remote Sens. 11, 22–24. https://doi.org/10.3390/rs11010031

El Hajj, M., Baghdadi, N., Zribi, M., Belaud, G., Cheviron, B., Courault, D., Charron, F., 2016. Soil moisture retrieval over irrigated grassland using X-band SAR data. Remote Sens. Environ. 176, 202–218. https://doi.org/10.1016/j.rse.2016.01.027

Engdahl, M.E., Borgeaud, M., Member, S., Rast, M., 2001. The Use of ERS-1 / 2 Tandem Interferometric Coherence in the Estimation of Agricultural Crop Heights. IEEE Trans. Geosci. Remote Sens. 39, 1799–1806. https://doi.org/0.1109/36.942558

Ezzahar, J., Ouaadi, N., Zribi, M., Elfarkh, J., Aouade, G., Khabba, S., Er-Raki, S., Chehbouni, A., Jarlan, L., 2020. Evaluation of Backscattering Models and Support Vector Machine for the Retrieval of Bare Soil Moisture from Sentinel-1 Data. Remote Sens. 12, 72. https://doi.org/10.3390/rs12010072

Ferrazzoli, P., Paloscia, S., Pampaloni, P., Schiavon, G., Solimini, D., Coppo, P., 1992. Sensitivity of microwave measurements to vegetation biomass and soil moisture content: a case study. IEEE Trans. Geosci. Remote Sens. 30, 750–756. https://doi.org/10.1109/36.158869

Fontanelli, G., Paloscia, S., Pampaloni, P., Pettinato, S., Santi, E., Montomoli, F., Brogioni, M., Macelloni, G., 2013. HydroCosmo: The monitoring of hydrological parameters on agricultural areas by using Cosmo-SkyMed images. Eur. J. Remote Sens. 46, 875–889. https://doi.org/10.5721/EuJRS20134652

Frison, P.L., Mougin, E., Hiernaux, P., 1998. Observations and Interpretation of Seasonal ERS-1 Wind Scatterometer Data over Northern Sahel (Mali). Remote Sens. Environ. 63, 233–242. https://doi.org/10.1016/S0034-4257(97)00137-5

Fung, A.K., Zongqian, L., Chen, K.S., 1992. Backscattering from a Randomly Rough Dielectric Surface. IEEE Trans. Geosci. Remote Sens. 30, 356–369. https://doi.org/10.1109/36.134085

Gherboudj, I., Magagi, R., Berg, A.A., Toth, B., 2011. Soil moisture retrieval over agricultural fields from multi-polarized and multi-angular RADARSAT-2 SAR data. Remote Sens. Environ. 115, 33–43. https://doi.org/10.1016/j.rse.2010.07.011

Greifeneder, F., Notarnicola, C., Hahn, S., Vreugdenhil, M., Reimer, C., Santi, E., Paloscia, S., Wagner, W., 2018. The Added Value of the VH/VV Polarization-Ratio for Global Soil Moisture Estimations from Scatterometer Data. IEEE J. Sel. Top. Appl. Earth Obs. Remote Sens. 11, 3668–3679. https://doi.org/10.1109/JSTARS.2018.2865185

Griffiths, G.H., Wooding, M.G., 1996. Temporal monitoring of soil moisture using ERS-1 SAR data. Hydrol. Process. https://doi.org/10.1002/(SICI)1099-1085(199609)10:9<1127::AID-HYP364>3.0.CO;2-#

Hagolle, O., Huc, M., Pascual, D.V., Dedieu, G., 2015. A multi-temporal and multi-spectral method to estimate aerosol optical thickness over land, for the atmospheric correction of FormoSat-2, LandSat, VENμS and Sentinel-2 images. Remote Sens. 7, 2668–2691. https://doi.org/10.3390/rs70302668

Hallikainen, M.T., Ulabz, F.T., Dobson, M.C., El-Rayes, M.A., Wu, L.K., 1985. Microwave Dielectric Behavior of Wet Soil-Part I: Empirical Models and Experimental Observations. IEEE Trans. Geosci. Remote Sens. GE-23, 25–34. https://doi.org/10.1109/TGRS.1985.289497

Holah, N., Baghdadi, N., Zribi, M., Bruand, A., King, C., 2005. Potential of ASAR/ENVISAT for the characterization of soil surface parameters over bare agricultural fields. Remote Sens. Environ. 96, 78–86. https://doi.org/10.1016/j.rse.2005.01.008

Hosseini, M., McNairn, H., 2017. Using multi-polarization C- and L-band synthetic aperture radar to estimate biomass and soil moisture of wheat fields. Int. J. Appl. Earth Obs. Geoinf. 58, 50–64. https://doi.org/10.1016/j.jag.2017.01.006

Jarlan, L., Khabba, S., Er-Raki, S., Le Page, M., Hanich, L., Fakir, Y., Merlin, O., Mangiarotti, S., Gascoin, S., Ezzahar, J., Kharrou, M.H., Berjamy, B., Saaïdi, A., Boudhar, A., Benkaddour, A., Laftouhi, N., Abaoui, J., Tavernier, A., Boulet, G., Simonneaux, V., Driouech, F., El Adnani, M., El Fazziki, A., Amenzou, N., Raibi, F., El Mandour, H., Ibouh, H., Le Dantec, V., Habets, F., Tramblay, Y., Mougenot, B., Leblanc, M., El Faïz, M., Drapeau, L., Coudert, B., Hagolle, O., Filali, N., Belaqziz, S., Marchane, A., Szczypta, C., Toumi, J., Diarra, A., Aouade, G., Hajhouji, Y., Nassah, H., Bigeard, G.,

Chirouze, J., Boukhari, K., Abourida, A., Richard, B., Fanise, P., Kasbani, M., Chakir, A., Zribi, M., Marah, H., Naimi, A., Mokssit, A., Kerr, Y., Escadafal, R., 2015. Remote Sensing of Water Resources in Semi- Arid Mediterranean Areas : the joint international laboratory TREMA. Int. J. Remote Sens. 36, 4879–4917. https://doi.org/10.1080/01431161.2015.1093198

Jarlan, L., Mazzega, P., Mougin, E., 2002. Retrieval of land surface parameters in the sahel from ERS wind scatterometer data: A "Brute force" method. IEEE Trans. Geosci. Remote Sens. 40. https://doi.org/10.1109/TGRS.2002.802500

Jarlan, L., Mougin, E., Frison, P.L., Mazzega, P., Hiernaux, P., 2002. Analysis of ers wind scatterometer time series over sahel (Mali). Remote Sens. Environ. 81, 404–415. https://doi.org/10.1016/S0034-4257(02)00015-9

Karam, M.A., Amar, F., Fung, A.K., Mougin, E., Lopes, A., Le Vine, D.M., Beaudoin, A., 1995. A microwave polarimetric scattering model for forest canopies based on vector radiative transfer theory. Remote Sens. Environ. 53, 16–30. https://doi.org/10.1016/0034-4257(95)00048-6

Karam, M.A., Amur, F., Fung, A.K., 1993. Electromagnetic Wave Scattering From a Forest or Vegetation Canopy : Ongoing Research at the University of Texas at Arlington. IEEE Antennas Propag. Mag. 35, 18–26.

Karam, M.A., Fung, A.K., Lang, R.H., Chauhan, N.S., 1992. Microwave Scattering Model for Layered Vegetation. IEEE Trans. Geosci. Remote Sens. 30, 767–784. https://doi.org/10.1109/36.158872

Kerr, Y., Waldteufel, P., Wigneron, J.P., Martinuzzi, J.M., Font, J., Berger, M., 2001. Soil Moisture Retrieval from Space: The Soil Moisture and Ocean Salinity (SMOS) Mission. IEEE Trans. Geosci. Remote Sens. 39, 1729–1735.

Kumar, K., Suryanarayana Rao, H.P., Arora, M.K., 2015. Study of water cloud model vegetation descriptors in estimating soil moisture in Solani catchment. Hydrol. Process. https://doi.org/10.1002/hyp.10344

Kumar, K., Suryanarayana Rao, H.P., Arora, M.K., 2014. Study of water cloud model vegetation descriptors in estimating soil moisture in Solani catchment. Hydrol. Process. 29, 2137–2148. https://doi.org/10.1002/hyp.10344

Le Hégarat-Mascle, S., Zribi, M., Alem, F., Weisse, A., Loumagne, C., 2002. Soil moisture estimation from ERS/SAR data: Toward an operational methodology. IEEE Trans. Geosci. Remote Sens. 40, 2647–2658. https://doi.org/10.1109/TGRS.2002.806994

Le Morvan, A., Zribi, M., Baghdadi, N., Chanzy, A., 2008. Soil moisture profile effect on radar signal measurement. Sensors 8, 256–270. https://doi.org/10.3390/s8010256

Li, J., Wang, S., 2018. Using SAR-derived vegetation descriptors in a water cloud model to improve soil moisture retrieval. Remote Sens. 10. https://doi.org/10.3390/rs10091370

Macelloni, G., Paloscia, S., Pampaloni, P., Marliani, F., Gai, M., 2001. The relationship between the backscattering coefficient and the biomass of narrow and broad leaf crops. IEEE Trans. Geosci. Remote Sens. 39, 873–884. https://doi.org/10.1109/36.917914

Malbéteau, Y., Merlin, O., Balsamo, G., Er-Raki, S., Khabba, S., Walker, J.P., Jarlan, L., Malbéteau, Y., Merlin, O., Balsamo, G., Er-Raki, S., Khabba, S., Walker, J.P., Jarlan, L., 2018. Toward a Surface Soil Moisture Product at High Spatiotemporal Resolution: Temporally Interpolated, Spatially Disaggregated SMOS Data. J. Hydrometeorol. https://doi.org/10.1175/JHM-D-16-0280.1

Mattia, F., Balenzano, A., Rinaldi, M., Steduto, P., Moreno, J., 2015. SENTINEL-1 FOR WHEAT MAPPING AND SOIL MOISTURE RETRIEVAL, in: 2015 IEEE International Geoscience and Remote Sensing Symposium (IGARSS). pp. 2832–2835. https://doi.org/10.1109/IGARSS.2015.7326404

Mattia, F., Le Toan, T., Picard, G., Posa, F.I., D'Alessio, A., Notarnicola, C., Gatti, A.M., Rinaldi, M., Satalino, G., Pasquariello, G., 2003. Multitemporal C-band radar measurements on wheat fields. IEEE Trans. Geosci. Remote Sens. 41, 1551–1560. https://doi.org/10.1109/TGRS.2003.813531

Ministre de l'agriculture et peche maritime du develpement rurale et des eaux et forets (Ed.), 2018. Agriculture en chiffres 2017. PLAN MAROC VERT.

Miranda, N., Meadows, P.J., Type, D., Note, T., 2015. Radiometric Calibration of S-1 Level-1 Products Generated by the S-1 IPF. ESA-EOPG-CSCOP-TN-0002; Eur. Sp. Agency Paris, Fr.

Mission, R.O., Services, G.O., 2012. ESA's Radar Observatory Mission for GMES Operational Services, SP-1322/1. ed.

Moran, S.S., Vidal, A., Troufleau, D., Qi, J., Clarke, T.R., Pinter, P.J., Mitchell, T.A., Inoue, Y., Neale, C.M.U., 1997. Combining multifrequency microwave and optical data for crop management. Remote Sens. Environ. https://doi.org/10.1016/S0034-4257(96)00243-X

Morrison, K., Bennett, J.C., Nolan, M., Menon, R., 2011. Laboratory Measurement of the DInSAR Response to Spatiotemporal Variations in Soil Moisture - IEEE Journals & Magazine. IEEE Trans. Geosci. Remote Sens. 49, 3815–3823. https://doi.org/10.1109/TGRS.2011.2132137

Naeimi, V., Scipal, K., Bartalis, Z., Hasenauer, S., Wagner, W., 2009. An improved soil moisture retrieval algorithm for ERS and METOP scatterometer observations. IEEE Trans. Geosci. Remote Sens. 47, 1999–2013. https://doi.org/10.1109/TGRS.2008.2011617

Nesti, G., Tarchi, D., Despan, D., Rudant, J.-P., Bedidi, A., Borderies, P., Bachelier, E., 1998. Phase Shift and Decorrelation of Radar Signal Related to Soil Moisture Changes Phase Shift and Decorrelation of Radar Signal. Proc. Second Int. Work. Retr. Bio- Geo-physical Parameters from SAR Data L. Appl. tions. Noordwijk, Netherlands ESA Publ. Div.

Njoku, E.G., 2004. AMSR-E/Aqua Daily L3 Surface Soil Moisture, Interpretive Parameters, & QC EASE-Grids, Version 2. Boulder, Colorado, USA. https://doi.org/https://doi.org/10.5067/AMSR-E/AE_LAND3.002

Nolin, M.., Quenum, M., Cambouris, A.., Martin, A., Cluis, D., 2005. Rugosité de la surface du sol – description et interprétation. Agrosol 16, 5–21.

Oh, Y., Sarabandi, K., Ulaby, F.T., 1992. An Empirical Model and an Inversion Technique for Radar Scattering from Bare Soil Surfaces. IEEE Trans. Geosci. Remote Sens. 30, 370–381. https://doi.org/10.1109/36.134086

Paloscia, S., Pettinato, S., Santi, E., Notarnicola, C., Pasolli, L., Reppucci, A., 2013. Soil moisture mapping using Sentinel-1 images: Algorithm and preliminary validation. Remote Sens. Environ. 134, 234–248. https://doi.org/10.1016/j.rse.2013.02.027

Paloscia, S., Santi, E., Fontanelli, G., Montomoli, F., Brogioni, M., MacElloni, G., Pampaloni, P., Pettinato, S., 2014. The sensitivity of cosmo-skymed backscatter to agricultural crop type and vegetation parameters. IEEE J. Sel. Top. Appl. Earth Obs. Remote Sens. 7, 2856–2868. https://doi.org/10.1109/JSTARS.2014.2345475

Periasamy, S., 2018. Significance of dual polarimetric synthetic aperture radar in biomass retrieval : An attempt on Sentinel-1. Remote Sens. Environ. 217, 537–549. https://doi.org/10.1016/j.rse.2018.09.003

Picard, G., Toan, T. Le, Mattia, F., 2003. Understanding C-Band Radar Backscatter From Wheat Canopy Using a Multiple-Scattering Coherent Model. IEEE Trans. Geosci. Remote Sens. 41, 1583–1591. https://doi.org/10.1109/TGRS.2003.813353

Picard, G., Toan, T.L., 2002. A Multiple Scattering Model for C-Band Backscatter of Wheat Canopies. J. Electromagn. Waves Appl. 16, 1447–1466. https://doi.org/10.1163/156939302X00093

Prevot, L., Champion, I., Guyot, G., 1993. Estimating Surface Soil Moisture and Leaf Area Index of a Wheat Canopy Using a Dual-Frequency (C and X Bands) Scatterometer. Remote Sens. Environ. 46, 331–339.

Rafi, Z., Merlin, O., Le, V., Khabba, S., Mordelet, P., Er-raki, S., Amazirh, A., Olivera-guerra, L., Ait, B., 2019. Partitioning evapotranspiration of a drip-irrigated wheat crop : Inter- comparing eddy covariance- , sap fl ow- , lysimeter- and FAO-based methods. Agric. For. Meteorol. 265, 310–326. https://doi.org/10.1016/j.agrformet.2018.11.031

Sano, E.E., Huete, A.R., Troufleau, D., Moran, M.S., Vidai, A., 1998. Relation between ERS-1 synthetic aperture radar data and measurements of surface roughness and moisture content of rocky soils in a semiarid rangeland. Water Resour. Res. https://doi.org/10.1029/98WR00032

Scott, C.P., Lohman, R.B., Jordan, T.E., 2017. InSAR constraints on soil moisture evolution after the March 2015 extreme precipitation event in Chile. Sci. Rep. 7. https://doi.org/10.1038/s41598-017-05123-4

Sieber, A.J., Kouyate, F., Fung, A.K., 1982. A Backscatter Model for a Randomly Perturbed Periodic Surface. IEEE Trans. Geosci. Remote Sens. GE-20, 518–528. https://doi.org/10.1109/TGRS.1982.350420

Small, D., 2011. Flattening Gamma : Radiometric Terrain Correction for SAR Imagery. IEEE Trans. Geosci. Remote Sens. 49, 3081–3093. https://doi.org/10.1109/TGRS.2011.2120616

Small, D., Schubert, A., 2008. Guide to ASAR Geocoding. ESA-ESRIN Tech. Note RSL-ASAR-GC-AD 1–36. https://doi.org/RSL-ASAR-GC-AD

Taconet, O., Benallegue, M., Vidal-Madjar, D., Prevot, L., Dechambre, M., Normand, M., 1994. Estimation of soil and crop parameters for wheat from airborne radar backscattering data in C and X bands. Remote Sens. Environ. 50, 287–294. https://doi.org/10.1016/0034-4257(94)90078-7

Tanji, A., 2005. Adventices du blé et de l'orge au Maroc. 'Institut National de la Recherche Agronomique Maroc, Rabat.

Torres, R., Snoeij, P., Geudtner, D., Bibby, D., Davidson, M., Attema, E., Potin, P., Rommen, B., Floury, N., Brown, M., Navas, I., Deghaye, P., Duesmann, B., Rosich, B., Miranda, N., Bruno, C., Abbate, M.L., Croci, R., Pietropaolo, A., Huchler, M., Rostan, F., 2012. GMES Sentinel-1 mission. Remote Sens. Environ. 120, 9–24. https://doi.org/10.1016/j.rse.2011.05.028

Touzi, R., Lopes, A., Bruniquel, J., Vachon, P.W., 1999. Coherence estimation for SAR imagery. IEEE Trans. Geosci. Remote Sens. 37, 135–149. https://doi.org/10.1109/36.739146

Ulaby, F., Moore, R., Fung, A., 1986. Microwave remote sensing active and passive-volume III: from theory to applications.

Ulaby, F.T., Allen, C.T., Iii, G.E., 1984. Relating the Microwave Backscattering Coefficient to Leaf Area Index. Remote Sens. Environ. 14, 113–133. https://doi.org/doi.org/10.1016/0034-4257(84)90010-5

Ulaby, F.T., Aslam, A., Dobson, M.C., 1982. Effects of Vegetation Cover on the Radar Sensitivity to Soil Moisture. IEEE Trans. Geosci. Remote Sens. GE-20, 476–481. https://doi.org/10.1109/TGRS.1982.350413

Ulaby, F.T., Batlivala, P.P., Dobson, M.C., 1978. Microwave Backscatter Dependence on Surface Roughness, Soil Moisture, and Soil Texture: Part I - Bare Soil. IEEE Trans. Geosci. Electron. 16, 286–295. https://doi.org/10.1109/TGE.1978.294586

Ulaby, F.T., Bush, T.F., 1976. Monitoring Wheat Growth With Radar. Photogramm. Eng. Remote Sensing 42, 557–568.

Ulaby, F.T., Sarabandi, K., McDonald, K., Whitt, M., Craig Dobson, M., 1990. Michigan microwave canopy scattering model. Int. J. Remote Sens. 11, 1223–1253. https://doi.org/10.1080/01431169008955090

Veloso, A., Mermoz, S., Bouvet, A., Le Toan, T., Planells, M., Dejoux, J.F., Ceschia, E., 2017. Understanding the temporal behavior of crops using Sentinel-1 and Sentinel-2-like data for agricultural applications. Remote Sens. Environ. 199, 415–426. https://doi.org/10.1016/j.rse.2017.07.015

Wagner, W., Lemoine, G., Borgeaud, M., Rott, H., 1999. A study of vegetation cover effects on ERS scatterometer data. IEEE Trans. Geosci. Remote Sens. 37, 938–948. https://doi.org/10.1109/36.752212

Walker, J.P., Houser, P.R., Willgoose, G.R., 2004. Active microwave remote sensing for soil moisture measurement: A field evaluation using ERS-2. Hydrol. Process. https://doi.org/10.1002/hyp.1343

Wang, H., Magagi, R., Goïta, K., 2018. Potential of a two-component polarimetric decomposition at C-band for soil moisture retrieval over agricultural fields. Remote Sens. Environ. 217, 38–51. https://doi.org/10.1016/j.rse.2018.08.003

Wegmuller, U., Werner, C., 1997. Retrieval of Vegetation Parameters with SAR Interferometry. IEEE Trans. Geosci. Remote Sens. 35, 18–24. https://doi.org/10.1109/36.551930

Zebker, H.A., Villasenor, J., 1992. Decorrelation in Interferometric Radar Echoes. IEEE Trans. Geosci. Remote Sens. 30, 950–959. https://doi.org/10.1109/36.175330

Zribi, M., Baghdadi, N., 2015. Potential of high spatial resolution radars for the characterization of soil properties in agricultural environments, in: Erlanger Geographische Arbeiten Band 42. pp. 33–52.

Zribi, M., Chahbi, A., Shabou, M., Lili-Chabaane, Z., Duchemin, B., Baghdadi, N., Amri, R., Chehbouni, A., 2011. Soil surface moisture estimation over a semi-arid region using ENVISAT ASAR radar data for soil evaporation evaluation. Hydrol. Earth Syst. Sci. 15, 345–358. https://doi.org/10.5194/hess-15-345-2011

Zribi, M., Dechambre, M., 2002. A new empirical model to retrieve soil moisture and roughness from C-band radar data. Remote Sens. Environ. 84, 42–52. https://doi.org/10.1016/S0034-4257(02)00069-X

Zribi, M., Hegarat-Mascle, S. Le, Ottle, C., Kammoun, B., Guerin, C., 2003. Surface soil moisture estimation using active microwave ERS wind scatterometer and SAR data. IGARSS 2003. 2003 IEEE Int. Geosci. Remote Sens. Symp. Proc. (IEEE Cat. No.03CH37477) 2, 5–7. https://doi.org/10.1109/IGARSS.2003.1294122

List of figure captions

Appendix 1: Backscattering model description

The canopy-backscattering coefficient is given as the incoherent sum of three contributions: the attenuated surface scattering from the underlying soil, the volume scattering from the canopy and the soil-vegetation multiple scattering interaction as follows:

$$\sigma^0_{pq,\ canopy} = \sigma^0_{pq,\ vegetation} + \sigma^0_{pq,\ soil-vegetation} + L^2\sigma^0_{pq,\ soil} \quad \text{(A1)}$$

Where pq is the polarization mode (V or H). $\sigma^0_{pq,\ vegetation}$, $\sigma^0_{pq,\ soil-vegetation}$ and $\sigma^0_{pq,\ soil}$ denote the contributions of vegetation, interactions soil-vegetation and bare soil, respectively. $L^2$is the two-way transmissivity factor of the canopy.

1. Oh Model

The contribution of the soil component was calculated using the Oh et al. model (1992). This model has been shown to be applicable to a large range of soil roughness conditions and a large range of incidence angle in various context (Frison et al., 1998; Jarlan et al., 2002). The soil backscattering coefficient is expressed as a function of one parameter related to the soil roughness (h_{rms}) only when compared to other models including IEM (Fung et al., 1992). Other input parameters are the angle of incidence (θ), the wave number (k) and the dielectric constant of the soil surface (ε_r). This latter was computed from soil moisture and soil texture using the empirical model proposed in Hallikainen et al. (1985). The Oh model expresses the co-polarized and cross-polarized ratio to compute the backscattering coefficient of three linear polarizations (HH, VV and HV/ VH) as follows:

$$\sigma^0_{VV,\ soil} = g * (\cos\theta)^3 * (\Gamma_V + \Gamma_H)/\sqrt{p} \quad \text{(A2)}$$

$$\sigma^0_{VH,\ soil} = q * g * (\cos\theta)^3 * (\Gamma_V + \Gamma_H)/\sqrt{p} \quad \text{(A3)}$$

Where

$$q = 0.23 * \left(1 - e^{(-k*h_{rms})}\right) * \sqrt{\Gamma_0} \quad \text{(A4)}$$

$$\sqrt{p} = 1 - e^{(-k*h_{rms})} * \left(\frac{2\theta}{\pi}\right)^{\frac{1}{3}*\Gamma_0} \quad \text{(A5)}$$

$$g = 0.7 * \left(1 - e^{\left(-0.65*(k*h_{rms})^{1.8}\right)}\right) \quad \text{(A6)}$$

Γ_V, Γ_H, and Γ_0 are the Fresnel coefficients given by the following expressions:

$$\Gamma_V = \frac{\varepsilon_r \cos\theta - \sqrt{\varepsilon_r - \sin^2\theta}}{\left(\varepsilon_r \cos\theta + \sqrt{\varepsilon_r - \sin^2\theta}\right)^2}, \Gamma_H = \frac{\cos\theta - \sqrt{\varepsilon_r - \sin^2\theta}}{\left(\cos\theta + \sqrt{\varepsilon_r - \sin^2\theta}\right)^2} \text{ and } \Gamma_0 = \left|\frac{1-\sqrt{\varepsilon_r}}{1+\sqrt{\varepsilon_r}}\right|^2 \quad \text{(A7)}$$

2. Water Cloud Model

The semi-empirical water cloud model (Attema and Ulaby, 1978) aims to predict the radar backscatter over vegetation canopies. It represents the vegetation canopy as a cloud of identical water droplets. Indeed, the dielectric constants of dry matter and dry air are much smaller than the dielectric constant of water and the vegetation cover is composed of more than 99% of air by volume. The main assumptions of the water cloud model are: (1) that the multiple scattering within the canopy volume can be neglected, and (2) that cloud height and density are proportional to the VWC. The model domain of validity covers a large range of frequencies (8-18 GHz) and of incidence angles (0-70°). It has been shown to perform well in a large range of vegetation conditions and frequencies for the direct prediction of the backscattering coefficient as well as for the retrieval of soil moisture content and AGB (Bai et al., 2017; Bindlish and Barros, 2001; Bousbih et al., 2017; El Hajj et al., 2016; Hosseini and McNairn, 2017).

In the Water Cloud Model, the $\sigma^0_{soil-vegetation}$ term (cf. Eq. A1) is neglected (Frison et al., 1998; L. Jarlan et al., 2002; Kumar et al., 2014). The problem is then equivalent to the first order solution of the radiative transfer equation through a weak medium. $\sigma^0_{vegetation}$ and L^2 are expressed as follows:

$$\sigma^0_{pq,\ vegetation} = A_{pq} V_1 cos\theta (1 - L^2) \quad \text{(A8)}$$

$$L^2_{pq} = e^{-2B_{pq} V_1 sec\theta} \quad \text{(A9)}$$

Where θ is the incidence angle and A_{pq} and B_{pq} are the model's coefficients that depend on the canopy type, sensor's frequency and polarization and on the incidence angle. The first coefficient is related to the contribution of the direct scattering from the vegetation while the second represents the attenuation of the underlying soil backscattering by the canopy. V_1 is a parameter describing the vegetation canopy dynamics.